University of Strathclyde

Strathclyde Institute of Pharmacy and Biomedical Sciences

Supramolecular Assemblies: a New Route to Controlled Drug Delivery and Scaffold for Tissue Engineering

By

Yasir Abdulkarim Jarad

A thesis presented in fulfilment of the requirements for the degree of Master of Philosophy in Pharmacy

2014

Declaration

This thesis is the result of author's original research. It has been composed by the author and has not been previously submitted for the examination which has led to the award of a degree.

Yasir Abdulkarim Jarad

1/ 9/ 2014

Acknowledgment

I would like to express my gratitude towards my supervisor, Dr. Dimitrios Lamprou, for always being available to give invaluable advice. I would not have done this without his support and patience. I also acknowledge my second supervisor, Dr. Andrew Urquhart, who greatly supported my progress.

I take this opportunity to deeply thank Dr. Philipp Seib for his help in the cell culture work.

I would also like to thank all students and colleagues in Lamprou's group, past and present, for their friendship, advice and cooperation. Also, I would like to thank all the staff members and technicians at Strathclyde University for their kindness all over the time.

Last but not least, I thank my family, my parents, brothers and sisters. Above all, it is my loving father, who deserves most of the credit of what I have achieved in my life. I have no words to thank him for his assistance, moral support and more than anything for his love. Finally, I owe my loving thanks to my wife, Karawan Jubair, and daughters, Mariam and Mayar. Without them I would not have had the willpower to complete this work, and for their love and encouragement I am incredibly thankful.

Abstract

Ionic self-complementary peptides can self-assemble into hydrogels similar in properties to the natural extracellular matrix. Hydrogels can be exploited as drug carriers and scaffolds for tissue engineering due to many reasons including their biocompatibility, biodegradability and physico-chemical properties. RADA16-I, for instance, is characterised by its ability to form stable β-sheet nanostructures.

The main focus of this project is to study the effect of anionic salts (Hofmeister series) on the self-assembly of RADA16-I hydrogel which could be used as a drug vehicle and as a scaffold to induce the differentiation of mesenchymal stem cells into adipogenic and osteogenic linages.

Hydrogels were prepared using different concentrations (e.g. 100, 300, 600 and 900 mM) of sulphate, citrate, phosphate monobasic, chloride, perchlorate, nitrate, thiocyanate and iodide sodium salts, and characterised by CD and FT-IR. The 600 mM concentration was chosen as the minimum effective concentration which induces self-assembly in order to avoid cytotoxicity of the salts upon the cells. The prepared hydrogels in the presence of sulphate and iodide sodium salts were further characterised by circular dichroism (CD), FT-IR spectroscopy and atomic force microscopy (AFM). The stability of RADA16-I under physiological conditions (pH around 7, temperature of 37°C) was explored. The release of quinine from the self-assembling hydrogels was measured using UV-spectroscopy. Finally, the impact of the hydrogels on murine mesenchymal (C3H10T1/2) stem cells was assessed in order to provide a non-invasive strategy to manipulate the differentiation of stem cells in the absence of chemical treatment with potential for tissue engineering applications.

The peptide (RADA16-I) was shown to assemble into β-sheet nanofibres with a diameter of 23.4 ±2.1 nm, 40.8±3.7 nm in the presence of sodium sulphate, and 32.8±2.2 nm with sodium iodide. The CD and FT-IR results revealed that sulphate anion exhibited kosmotropic (gel maker) properties while and iodide acted as a chaotrope (gel breaker). The stability experiment showed that RADA16-I lost its β-nanostructures at a pH around 7 and formed irregular aggregates indicating that the self-assembly of this peptide occurs in acidic environments rather than the physiological pH.

Quinine release decreased with the kosmotropic sulphate system compared with the chaotropic iodide indicating that salt-induced self-assembling peptides can be used as vehicles for controlled drug release.

Fibronectin (FN) was used to enhance the cell attachment on the hydrogel. The cell culture findings suggested that inducing the self-assembly of peptide hydrogels by ionic salts might not be a suitable strategy for using hydrogels in the biomedical applications of murine C3H10T1/2 stem cells due to the cytotoxicity of the sulphate and iodide ions on the cells.

Table of contents

List of abbreviations

A	Alanine
AFM	Atomic force microscopy
ALP	Alkaline phosphatase activity
BCA	Bicinchoninic acid assay
BFGF	Basic fibroblast growth factor
BMP4	Bone morphogenetic protein4
BNDF	Brain-derived neurotrophic factor
CBZ	Carboxybenzyl
CD	Circular dichroism
CDNN	Circular dichroism spectra deconvolution software
2D	Two dimension
3D	Three dimension
D	Aspartic acid
DMEM	Dulbecco's modified eagle medium
DMSO	Dimethyl sulphoxide
DMT Modulus	Derjagin, Muller, Toropov (Young's) modulus
DNA	Deoxyribonucleic acid
DSC	Differential scanning calorimetry
E	Glutamic acid
ECM	Extracellular matrix
F-F	Diphenylalanine
Fmoc	Fluorenylmethyloxycarbonyl
FN	Fibronectin
FT-IR	Fourier transform infrared spectroscopy

HPLC	High performance liquid chromatography
HS	Hofmeister series
HTCC	N-(2-hydroxy)propyl-3-trimethyl ammonium chitosan chloride
IBMX	3-Isobutyl-1-methylxantihine
IGF-1	Insulin-like growth factor 1
MALLS	Multi-Angle Light Scattering
MTT	MTT ((3-(4, 5-dimethylthiazol-2-yl)-2, 5-diphenyltetrazolium bromide)
NMR	Nuclear magnetic resonance spectroscopy
OSM–PCLA–PEG–PCLA–OSM	Oligomeric sulphamethazine-poly(epsilon-caprolactone-co-lactide)-poly(ethylene glycol)- poly(epsilon-caprolactone-co-lactide)-oligomeric sulphamethazine
PEG	Polyethylene glycol
PFA	Paraformaldehyde
PF-QNM	Peak force-quantitative nanomechanical mapping
PFT	Peak force tapping
PHEMA	Poly-hydro hydroxyethylmethacrylate
RNA	Ribonucleic acid
Q	Glutamine
QNM	Quantitative Nanomechanical Property Mapping
R	Arginine
SD	Standard deviation
TMAFM	Tapping (intermediate contact) mode
UV	Ultraviolet
VEGF	Vascular endothelial growth factor

List of figures

List of tables

Chapter one: Literature review

1.1 Introduction

Living systems are structurally based on highly-organised supramolecules, for instance DNA, RNA, proteins and polysaccharides. These structures hierarchically result from smaller molecules (e.g. nucleotides, amino acids and monosaccharaides) that join together via non-covalent bonds to form polymers [1]. Similarly, organs are formed by tissues which are composed of cells.

Inspired by such concepts, scientists have developed soft materials with designed characteristics that can be exploited in particular biomedical applications such as drug delivery [2] and tissue engineering [3]. Peptide hydrogels and their constitutive monomers have been widely used in such applications depending upon their ability to self-assemble in response to external stimuli.

Ionic complementary peptides are amphiphilic macromolecules that can assemble to create nanoscale β-sheet fibres in aqueous media or biological fluids through hydrogen bonding, van der Waals and other interactions [4].

RADA16-I hydrogel, an amphiphilic ionic complementary peptide, has attracted great attention in a wide range of biomedical applications as it can form nanoscale matrices that mimic the extracellular matrix of tissues and also as a drug delivery system .

The biomedical applications of RADA16-I as a tissue scaffold and drug carrier in the literature will be reviewed in this chapter. The previous studies discussed the self-assembly of this hydrogel under different conditions such as pH and conjugation with motifs [5-11], however, the influence of ionic salts on RADA16-I self-assembly has not been covered. Therefore, the primary focus of this project is to explore the effect of

different ionic salts on the supramolecular self-assembly of RADA16-I aimed at creating scaffolds to investigate the impact of the new systems upon the linage differentiation of murine mesenchymal stem cells as well as drug release profile.

1.2 Hydrogels

Since Wichterle and Lim, Czechoslovakian scientists, published their first report on synthetic hydrogels in 1960 [12], the research of hydrogels and technologies have developed significantly due to their widely used applications in many industrial and biomedical fields such as drug carriers, scaffolds for tissue engineering and absorbents for chemicals [13]. This importance and phenomenal growth can be noticed from the number of publications (reviews, journals, reports, conferences and books) reported every year [14]. Hydrogels (or hydrogelators) are hydrophilic three-dimensional polymeric materials, cross-linked via physical or chemical interactions, and capable of entrapping large amounts of water without dissolving [15]. They show an intermediate behaviour between solid and liquid materials. Cross-links between their monomers make them insoluble in water and also provide desired mechanical support, physical stability and structural strength to the hydrogels [3]. Hydrogels effectively respond to different external stimuli such as salts, solvents, pH, temperature, enzymes, electromagnetic radiation, and electrical field. For example, the azo-dipeptide “Azo-Ala-Tyr” forms a gel at pH 7 [16], while Boc-Val-Pro-Arg-MCA peptide is thrombin-sensitive [17]. Such responses can be utilised by researchers depending on their goals. The appropriate selection of starting constituents, synthesising techniques and conditions are vital to

design a hydrogel for a specific purpose as all these aspects have direct impacts on its properties and behaviour in biological systems [18]. Recent innovations in nanotechnology techniques, such as atomic force microscopy (AFM), have accelerated this trend [19].

1.2.1 Hydrogel classification

Hydrogels can be classified depending upon the origin of building blocks, method of synthesis, physicochemical properties, degree of swelling, porosity, physical structure, ionic charges, and biodegradability [20]. Based on the origin, hydrogels are natural, synthetic or prepared from both synthetic and natural materials to gain combined features in one hydrogel [20]. Polysaccharides (e.g. hyaluronic acid) and proteins (e.g. collagens) are examples of natural monomers which can be obtained from an animal or plant source and modified to generate hydrogels [21]. Poly (hydroxyl cellulose), poly (acrylic acid), poly (acrylamide) and polypeptide hydrogels are examples in the synthetic category [22]. Cross-linking type is another criterion which can be used to classify hydrogels. In chemical cross-linked hydrogels, the polymeric chains are covalently cross-linked i.e. irreversible junctions which cannot be reshaped easily. By contrast, physically cross-linked hydrogels have non-covalent (transient) junctions such as hydrogen bonds, electrostatic interactions, hydrophobic associations and others. Such interactions are reversible, therefore; physical hydrogels can be generated in response to external stimuli, for instance temperature and solvents, which induce the self-assembly of polymers [23]. Hydrogels can also be grouped on the basis of preparation approach into homo-polymer, copolymer and multi-polymer. Homo-polymer hydrogels contain a single type of

building block (monomer). Copolymers are polymers derived from two species of monomers, while multi-polymers are hydrogels composed of more than three types of monomers. Furthermore, polymeric hydrogels are neutral, cationic, anionic or amphiphilic depending on the ionisable groups [24].

1.2.2 Hydrogel structures and properties

Understanding the structure-property relationship of a required polymeric hydrogel is essential in deciding which building blocks are suitable for the desired application, since the mechanical stress, swelling ability and other physical properties of hydrogels are in fact the properties of their constitutive materials [25]. The swelling behaviour, cross-linking density and degradability properties of hydrogels are extremely important for hydrogelators synthesis [20].

Since hydrophilic (most polar) moieties in hydrogels absorb water first (primary bound water), the hydrogels swell. The swelling exposes the lipophilic parts and then leads to more water absorption due to osmosis (secondary bound water). The primary and secondary water are called "total bound water" [26]. "Bulk water" is a term used to describe the amount of water absorbed by hydrogels when both hydrophilic and hydrophobic groups become saturated which leads to further swelling [27]. The ability of a polymeric hydrogel to absorb water and swell is related to the degree of cross-linking (bond strength) between its monomers. The swelling-equilibrium state is reached when the swelling force and its counterbalancing force, the cross-links, become equal [28]. Viscoelastic modulus and swelling equilibrium state are used to measure the degree of

cross-linking, while polymer volume fraction in swollen state, weight of a hydrogel before and after the swelling (swelling ratio) and network mesh size are three important parameters utilised to understand the swelling kinetics and structure of hydrogels [29]. In addition, mechanical strength, stress-strain behaviour and permeability are closely related to the cross-linking density.

Surface properties must also be taken into account in the designing of polymeric hydrogels. Hydrogel surfaces are highly complex with numerous ionisable groups and semi-mobile chains which are attached from one side to the back-bone network. These ionisable groups and dangling chains are particularly important in the cell adhesion process with tissue scaffolds. Also, they control the self-assembly when hydrogels are mixed with solvents [30].

1.2.3 Hydrogels in drug delivery and tissue engineering

The physicochemical properties of hydrogels have made them unique in many areas including industrial, pharmaceutical and biomedical [31]. Wound healing, soft contact lenses, absorbents, implantable bio-devices and biosensors are examples of the potential applications of hydrogels [31]. For instance, Poly-hydro hydroxyethylmethacrylate (pHEMA) hydrogels are used widely in soft contact lenses manufacturing as well as carriers for many ocular drugs [32]. Chen *et al.* prepared a peptide hydrogel containing light-sensitive chromophores which can exhibit energy transfer reaction. This hydrogel can be used as a light-harvesting biomaterial [33]. In recent years, the use of hydrogels in

tissue engineering, regenerative medicine and in drug delivery has been given particular attention [34].

Regenerative medicine is a new core-discipline of modern health care. In the last two decades, there has been a growing interest in regenerative medicine not only from scientists and physicians but also from society for understanding what regenerative medicine can afford in terms of new therapies and ways to manage diseases [35]. Tissue engineering and regenerative medicine aim to restore or maintain normal function of tissues and organs having defects or dysfunctions; they may involve the regeneration of entire organs [36]. In 2008, Macchiarini *et al.* succeeded in replacing the trachea of a patient with bronchomalacia with a decellularised trachea seeded with mesenchymal stem cells [37]. Song *et al.* bioengineered a kidney from scaffolds of a rat's kidney *in vitro* where the new transplanted grafts were able to produce urine *in vivo* [38].

The key idea of tissue engineering is how to induce living cells to form tissues and to carry out the functions of those tissues. Tremendous advances in cell biology, genetics and biomaterials have totally revolutionised this field and generated unusual opportunities to fabricate tissues *in vitro* [39].

As the role of hydrogels in tissue engineering is generally to provide scaffolds for incorporated cells, the scaffolds should act as transient extracellular matrices (ECM) until cells build their own ECM, and therefore; hydrogels have to be biodegradable to avoid surgical interventions to remove them. Moreover, they have to be mechanically strong enough to prevent cells from floating out of the targeted organs and to facilitate cell proliferation and migration which can be enhanced by adding growth factors into gels.

Additionally, scaffolds have to have a good permeability for influx and efflux of nutrients and metabolites. In tissue engineering, hydrogelators can be either created *in vitro* then implanted in the body or injected directly as a liquid that converts to the gel state *in situ* [13]. In a study published by Amosi *et al.,* a peptide hydrogel containing a high percentage of aspartic acid and tricalcium phosphate induced osteoblast differentiation and showed good bone defect healing in mouse distal femurs [40].

Potential applications of hydrogels in drug delivery arise from their ability to respond to external stimulation. Monomers of hydrogels used for drug delivery purposes are *in-situ* stimuli-sensitive [13]. They show sol-gel volume transition, and such a characteristic has many advantages, simple formulation requirements, organ-specificity and controlled release behaviour [29]. Furthermore, hydrogels are good carriers for hydrophilic and lipophilic drugs [41]. Drug molecules are released when hydrogels swell *in vivo* and dissolute due to different stimuli such as temperature and pH. Amphiphilic polyethylene glycols (PEGs) are widely applied in drug delivery. Poly(N-isopropylacrylamide), Poly(N-vinylisobutyramide), chitosan, Pluronics and poly(organophosphazenes) are thermo-sensitive PEG hydrogel examples [42-44]. Wu *et al.* synthesised a hybrid hydrogel by mixing PEG with a chitosan derivative "N-(2-hydroxy) propyl-3-trimethyl ammonium chitosan chloride (HTCC)" for nasal drug delivery of insulin in rats. The applied solution showed thermal transition from solution (at room temperature) to hydrogel (at body temperature in the nasal cavity), and insulin absorption was demonstrated by the significant decrease in the concentration of blood glucose [45].

The pH-sensitive amphiphilic hydrogels are also attractive, since they have considerable advantages over thermo-sensitive hydrogels; early gelation in thermo-gelling based

hydrogelators is avoidable, and they are easier to be stored in contrast to thermo-sensitive systems. The pH-sensitive hydrogels are either basic or acidic weak polyelectrolytes, such as oligomeric sulphamethazine-poly(epsilon-caprolactone-co-lactide)-poly(ethylene glycol)- poly(epsilon-caprolactone-co-lactide)-oligomeric sulphamethazine OSM–PCLA–PEG–PCLA–OSM (Figure 1) and poly (tertiary amine methacrylate) hydrogels [7]. An example on this type is a novel hydrogel designed by Mahkam *et al.* for large-intestine specific drug delivery; the prepared copolymer (acryloyl-cubane dicarboxylic acid-hydroxyethyl methacrylate) enhanced the release and absorption of an azo prodrug of the anti-inflammatory 5-amino salicylic acid due to the pH environment of the large intestine [46].

With regard to drug delivery applications, particular attention has been devoted to combined amphiphilic hydrogels having multifunctional groups and mutisensitive features. These systems can be injected deep in the body and show sustained release behaviour. They also provide a suitable environment for some sensitive biomolecules such as DNA and proteins [47]. A novel double-sensitive poly(ester amino urethane)$_n$ (PCL–PEG–PCL–PAU) hydrogel is synthesised by combining both thermo-sensitive and pH-sensitive polymers [48].

Hydrogel coatings have been recently developed and used for drug delivery purposes [49]. Di Giglio *et al.* synthesised a hydrogel composed of 2-hydroxyethyl methacrylate, poly (ethylene glycol diacrylate) and acrylic acid. This hydrogel was loaded with ciprofloxacin and used as a coating material on titanium surfaces and evaluated against methicillin resistant *Staphylococcus aureus* [49].

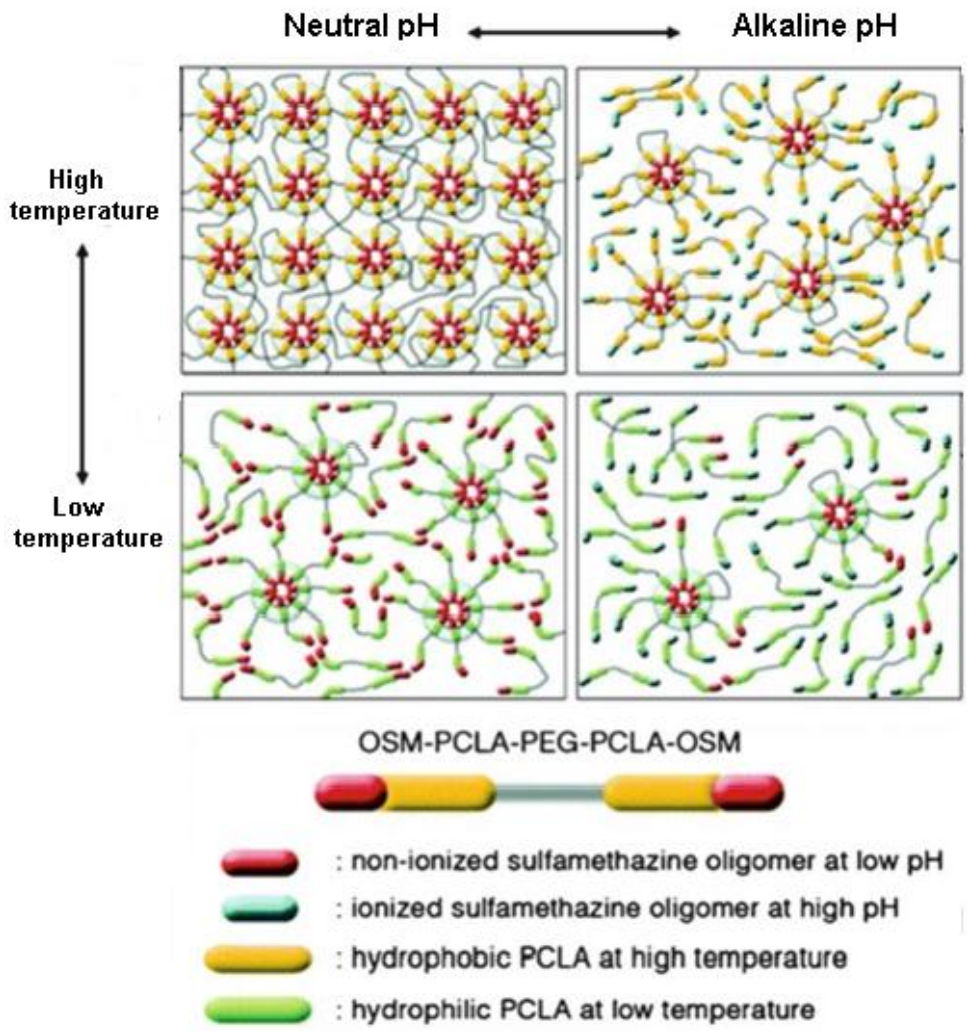

Figure 1 Sol–gel transition of the pH and temperature sensitive OSM–PCLA–PEG–PCLA–OSM hydrogel, adapted from [31].

Since this research study is mainly focus on peptide-based hydrogels, detailed discussion of this category will be given in the following section.

1.3 Peptide-based hydrogels

1.3.1 Introduction to peptide-based hydrogels

Understanding the basic structure of amino acids, peptides and proteins represents the starting point to understand their physico-chemical properties and biological effects. Peptides are short polymers composed of short chains of amino acids linked by peptide (covalent) bonds which form between the amino group of one amino acid and the carboxyl functional group of another. Peptides may contain up to 50 amino acids [1]. All amino acids have the same basic structure (Figure 2); a hydrogen atom, a carboxylic group, an amino group and a side chain (R) attached to one carbon atom called the "α-carbon". Nevertheless, they differ in their side chains. Amino acids are categorised based on the nature and properties of the side chains, which affects their physico-chemical properties, into charged, neutral, hydrophobic, hydrophilic and others [1].

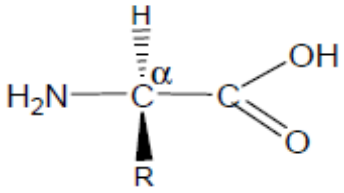

Figure 2 Basic chemical structure of amino acids

The structure of peptides and proteins is classified into four levels; primary, secondary, tertiary and quaternary. **The primary structure** is related to the amino acid sequence in the chain where peptide bonds are formed between the C-termini and N-termini of amino acids.

The secondary structure (Figure 3) refers to the most energetically favoured three-dimensional (3-D) structural conformation of a biopolymer which is caused by the local folding within the polypeptide chain as a result of intramolecular hydrogen bonds formed between backbone (-NH) and (-COOH) functional groups. There are various secondary structures, for instance α-helix, β-sheet, turns and random coils. In α-helix (coils) structures, the biopolymer chain folds in a right-hand or left-hand screw pattern. For each turn, the intramolecular hydrogen bonds are formed between the carboxyl oxygen of an amino acid and the amine hydrogen of a 3.6 residue away amino acid. In β-sheet (flat) structures, the hydrogen bonds are perpendicular to the polypeptide chain direction where these bonds can be generated between different segments of the same chain that is doubled back on itself or between different peptide chains. There are two possible forms of β-sheet; antiparallel and parallel sheets. The parallel configuration is less stable than the antiparallel configuration. Beta sheet structures are more rigid and less flexible than α-helix structures [50].

The tertiary structure corresponds to the 3-D arrangement of α-helices and β-sheets. These chains are stabilised by not only hydrogen bonds but also by hydrophobic, covalent disulphide, van der Waals interactions, ionic and other forces which are formed between the side chains (R) of different amino acids. The highest structural level of polypeptides and proteins is the "**quaternary structure**" which refers to the assembly of individual polypeptide chains or subunits to form a final specific shape. The quaternary structures are stabilised by the same interactions involved in the tertiary structures.

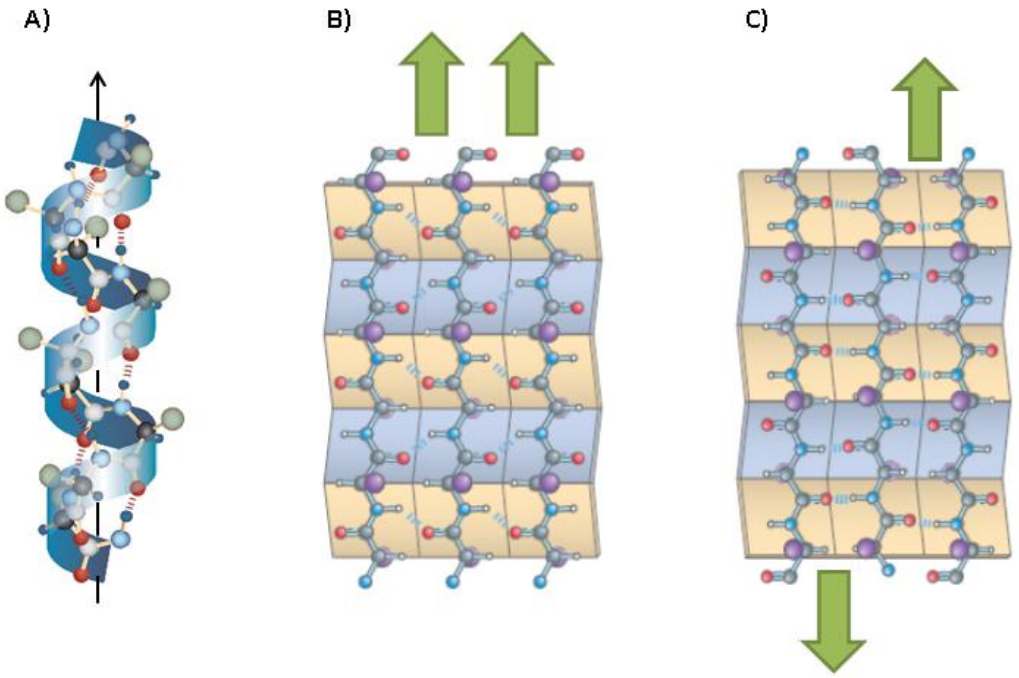

Figure 3 Secondary structure: A) α-helix, B) parallel β-sheet, C) anti parallel β-sheet, adapted from [1].

1.3.2 Properties of peptides that can assemble to form hydrogels

Several prerequisites of typical peptide-based hydrogels must be controlled to induce the self-assembly of these peptides to form hydrogels. The peptides must be partly insoluble and partly soluble in the chosen solvent(s). If the molecule is highly soluble it will dissolve while if it is highly insoluble it will precipitate. Also, they must be able to form multiple non-covalent associations with themselves such as hydrogen bonds, hydrophobic, electrostatic, π-stacking and others. These associations must be directional to specific regions in the polypeptide chains since their composing amino acids exhibit various assembly features [51]. Additionally, the stereochemistry of polypeptides at the molecular level must be well understood. The intrinsic chirality of peptide structures, α-helices and β-sheets, and their composing amino acids, L and D isomers, play a

significant role in directing the self-assembly at the nanoscale level [52]. Furthermore, many functional groups, for example carbonyl, amine, amide and sulphhydryl and aromatic rings, groups are contained within the side chains (R) in addition to the reactive moieties at the C- and N- termini of amino acids. These functional groups have the potential to form nanostructures, such as vesicles, instead of hydrogels [53]. An example of this phenomenon is the amino acid "diphenylalanine" (Figure 4c) which can form nanotubes. Reches *et al.* demonstrated the ability of aromatic peptides to form various nanostructures [54]. Therefore, various protecting groups can be used to prevent the nonspecific reactions of these moieties such as carboxybenzyl (CBz) (Figure 4a), fluorenylmethyloxycarbonyl (Fmoc) (Figure 4b) and allyloxycarbonyl groups [55].

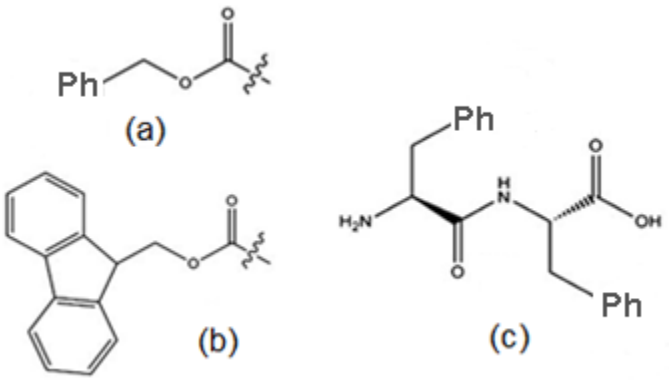

Figure 4 Structures of (a) CBz, (b) Fmoc, (c) diphenylalanine without a protecting group on the N-terminus, adapted from [56].

One further point to be considered is the concentration of the peptide which is very important in the self-assembly of different peptide-based hydrogels. Many researchers have reported the direct effect of peptide concentration on the gelation time, intermolecular interactions, network size and structure [57-59].

Aggeli *et al.* [60] reported the effect of the concentration on the self-assembly behaviour of P11-I (CH3COQQRQQQQQEQQ-NH2) peptide. Different concentrations resulted in different molecular architectures.

1.3.3 Self- assembly of peptide-based hydrogels

The wide range of applications of peptide-based hydrogelators as biomaterials is based on the fact that they can self-assemble into ordered arrangements and also undergo liquid-gel transition. Molecular self-assembly phenomenon is a reversible, autonomous process, involving the arrangement of building blocks into precisely defined, highly ordered and thermodynamically stable architectures [61]. The principle of this process is based on various types of physical, non-covalent, intramolecular and intermolecular associations such hydrophobic, hydrogen-bonding, pi-pi (π-π) stacking, van der Waals and electrostatic interactions [61]. Given the growing interest in self-assembly in biomedical research, different systems, hypotheses and models have been developed to understand the underlying molecular mechanism of this process and factors affecting it such as surfactant peptide systems [62, 63], coiled-coil peptide systems [64, 65], π-π stacking systems [66, 67], and β-hairpin peptide systems [68, 69]. Zhan's group was one of the first researchers to describe the self-assembly of peptides [70]. Ionic complementary peptides are a part of Zhang's system, and as RADA16-I (an ionic-complementary peptide) is the hydrogel used in this study, this system will be discussed in the following section.

1.3.3.1 Types of self-assembling systems

According to Zhang and his co-workers, [70-72], self-assembling systems of short, low molecular weight, peptides are grouped into five types. In **type I** or ‘‘molecular Lego’’ or “ionic complementary”, peptides assemble to form β-plate nanostructures in aqueous media or biological fluids due to the amphiphilic behaviour of their residues which enables them to create alternative complementary ionic interactions on the hydrophilic moiety. RADA-16 amphiphilic peptide is an example of this type [72]. **Type II** or ‘‘molecular switch’’ refers to the self-assembling peptides that undergo molecular structural change in response to external stimuli such as pH and temperature. A good example of these peptides is DAR16-IV which has a β-sheet arrangement at normal temperature while at high temperature the structure change to α-helices [72]. **Type III** or “molecular paint and carpet’’ peptides, such as RADSC-14 and RADSC-16, do not undergo intermolecular self-assembly [73]. However, they self-assemble onto surfaces creating monolayers which can interact with or attract other molecules. This system has useful applications in tissue engineering and cell biology [72]. **Type IV** refers to surfactant-like peptides that can form different nanostructures such as nanotubes. These biphasic peptides have two distinctive parts; a polar hydrophilic head and a non-polar hydrophobic tail. This system can be used as a gene, drug or protein delivery system [71]. Also, it can be considered as a good alternative for lipid-based surfactants. EAK16-IV, KAE16-IV and DAR32-IV are examples of this type. **Type V** is another system that has been developed by Zhang and his group. These systems consist of peptide and polymer segments which provide scaffolds to enhance bio-mineralisation [74].

Inter and intramolecular interactions represent the driving force of the self-assembly phenomenon. Thus, understanding the nature of these interactions is a central concern in this process. The next section will consider these interactions, their properties and the importance in self-assembly.

1.3.3.2 Forces that control self-assembling formation

The interactions controlling self-assembly are weak on their own to support the system, but collectively they can form stable well-defined structures. For example, the strength of typical covalent bonds is from 40 to 100 Kcal.mol^{-1} compared to 0.1 to 5 Kcal.mol^{-1} for hydrogen and van der Waals interactions [61]. Many amino acids contain lipophilic hydrocarbon side chains. The lipophilic side chains are either aliphatic or aromatic. The aliphatic side chains can be involved in hydrophobic interactions while the aromatic residues can form interactions via π-π stacking [75]. **The hydrophobic interactions** are generated to minimise the contact of hydrophobic side chains with the aqueous polar media since these residues are unable to create hydrogen bonds with water [61].

Aromatic π-π stacking interactions occur between π-electron donor and π-electron accepter aromatic components [76]. This type can be seen in π-conjugated systems, such as benzene rings, owing to the overlapping of *P*-orbitals. Short peptides containing aromatic residues can form stable β-sheet structures via hydrogen bonding and π-π stacking, for example the hydrophobic dipeptide diphenylalanine (F-F). Interestingly, aromatic protecting groups, such as Fmoc and CBz, that are added to protect N-termini from nonspecific interactions, provide a good environment to form π-π stacking

associations and thereby stable antiparallel β-sheets structures [77]. Yang *et al.* explained the effect of aromatic (R) side chain of amino acids on the elasticity of different hydrogels. According to this study, gel strength and elasticity can be improved by replacing aliphatic side chains by phenyl groups [78].

Hydrogen bonds are non-covalent electromagnetic attractive forces form between the hydrogen of proton donor electronegative atoms (such as O, N, and F) and proton acceptor chemical groups or electronegative atoms. Recently, several publications have focused on the formation of hydrogels from dipeptides in non-hydrogen boding solvents i.e. hydrophobic systems in order to decrease the unfavourable competition between the peptides and solvents towards the formation of hydrogen bonds [70]. Xu *et al.* suggest that the carboxylic groups of building blocks (amino acids) become protonated due to the hydrophobic environment [79].

Van der Waals (dipole-dipole) interactions are intermolecular attractive and repulsive forces occur between close molecules [80]. In fact, these molecules are electrically neutral; however, the unequal distribution of electrons surrounding their nuclei forms dipole moments (or dipoles) resulting in the attraction of the oppositely charged dipoles of the unbounded molecules. In **electrostatic interactions**, the attraction occurs between oppositely charged molecules or particles, for example carboxylic and amine groups of amino acids, while molecules with similar electric charges repel. These interactions are moderately strong in vacuum; nevertheless, they are weak in ionic solutions, such salts, since the salt ions shield the charged groups of the molecules weakening the interactions [50].

1.3.3.3 Synthetic approaches of self-assembly

The synthetic strategies of self-assembling peptide-based hydrogels can be classified into two general approaches; “Top-Down” and “Bottom-Up” [81]. In “Top-Down” systems, basic structures are built first then modified with different molecules, such as amino acids or other additives, which induce the self-assembly to form hydrogels. For example, Fmoc-Phe was used by Liu *et al.* to make films by using electrochemistry where the self-assembly could be disturbed by reversing the polarity of electrodes [82]. By contrast, in “Bottom-Up” systems, the additives are incorporated in the basic structures; the systems are then triggered by various stimuli, for instance pH, ionic salts and temperature, to form hydrogels [83]. Bottom-up systems are promising in developing novel soft materials with multi-functionalities which can control the molecular self-assembly [84]. As this study has been designed to investigate the effect of ions “Hofmeister series” on the self-assembly of RADA16-I hydrogel, the next point will discuss this phenomenon.

1.3.3.4 Hofmeister series

The Hofmeister (or lyotropic) series is a term used to classify ions according to their effect on protein aggregation and folding [148]. Ions, such as I^- and SCN^-, which tend to destabilise proteins and cause “salting-in” effects are called chaotropes or "water structure breakers". On the other hand, ions that stabilise folded proteins and cause “salting-out” effect are called kosmotropes or "water structure makers" such as $SO4^{-2}$ and $H2PO^{-4}$ [148]. This series was firstly identified in 1888 by Franz Hofmeister who noticed the ability of some inorganic salts to precipitate egg white protein more than others [146].

This effect has also been observed in polymer, colloid and surface science [121]. Specific ion effects upon peptides and proteins are important and have many applications in biology and chemistry such as enzyme performance [144], protein and peptide crystallisation [145], and microbiological growth [146]. This phenomenon is more noticeable in anions than cations [147]. The classic explanation of the influence of ions on the assembly of amino acids relies on two theories; the ability of water to form hydration shells around the ions, and the potential of the ions to alter the bulk water structure [142]. However, the specific ion effects cannot be understood by these hypotheses only, thus, the direct interactions between the ions and macromolecules provide more details about such effects [148]. From a thermodynamic point of view, a self-assembly pattern in the presence of an anion is thermodynamically more favourable than other conformations as systems tend to be in an equilibrium state (low enthalpy (*H*) and high entropy (*S*)) according to Gibbs free energy formula ($G= H-TS$), T is the absolute temperature [142] .

1.4 RADA16-I: a low molecular weight peptide for biomedical applications

1.4.1 Basic structure of RADA16-I

RADA16-I is a synthetic amphiphilic oligopeptide. It consists of sixteen amino acid residues. The basic structure contains three amino acids namely; arginine (R), alanine (A) and aspartic acids (D), Figure 6. The peptide sequence is [COCH3]-RADARADARADARADA-[CONH2] [77]. According to Zhang's systems, RADA16-I

belongs to Type I or “Ionic-complementary” subclass "Modulus I" (+ - + - + - + -) depending on the surface charge [section 1.3.3.1]. It can self-assemble to form stable β-plate secondary structures in water solutions depending on pH [85].

The alternating arrangement of charged segments, due to hydrophilic (R) and (D) amino acids, and the presence of hydrophobic moiety (A) make it organise in aqueous media in a two-face conformation (Figure 5) where (R) and (D) face the hydrophilic direction and (D) faces the hydrophobic direction [4].

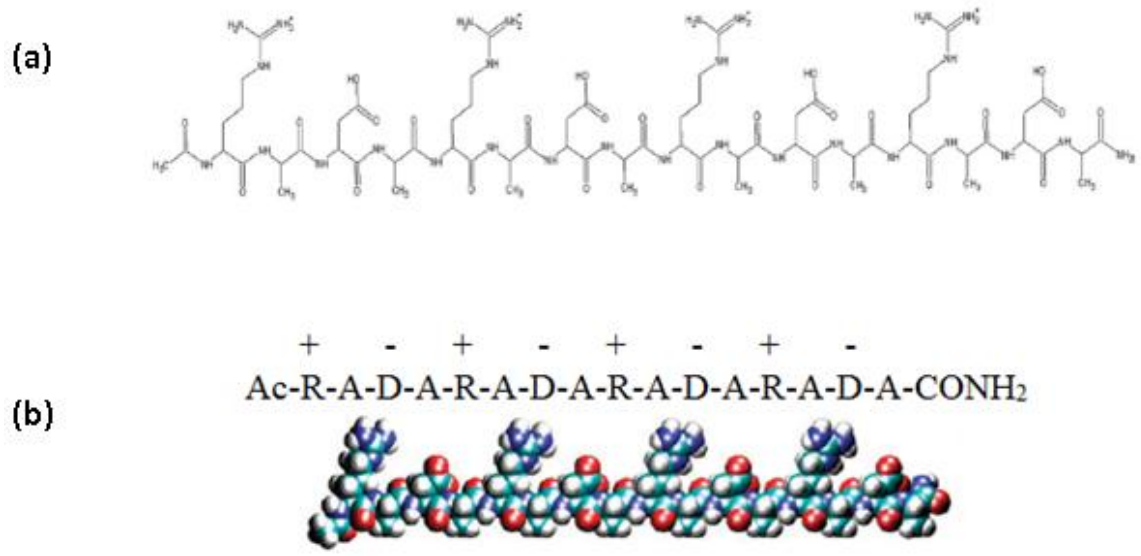

Figure 5 Chemical structure of RADA16-I, (a), and 3-D molecular model of RADA16-I. (b), It has 2 faces; polar hydrophilic (arginine R and aspartic acid D) and nonpolar hydrophobic (alanine A).

1.4.2 Biomedical applications of RADA16-I

Biomaterials are interactive substances capable of forming interactions with living tissues without causing harmful adverse effects. Due to their flexibility and high water content,

peptide-based hydrogels have been considered important biomaterials for pharmaceutical and other biomedical applications. New hydrogel systems with novel characteristics will continue to play a pivotal role in tissue engineering and drug delivery fields [86]. From a practical point of view, the growing interest in peptide-based hydrogelators as biomaterials is based on two main reasons. Their structural and other physical properties can be tuned and modified easily in order to suit the required application. Also, they are responsive to a wide variety of external stimuli or "triggers" which induce their self-assembly and sol-gel transitions [35].

RADA16-I exhibits reasonable interactions with living systems under the physiological conditions. It has many vital criteria that enable it to be an attractive peptide for biomedical applications. It can be chemically designed and tuned for specific requirements. Moreover, it is biocompatible due to the high water content, mechanical flexibility and the lack of cytotoxicity, pathogenicity, inflammatory or immune responses. In addition, it dissolves in water and biological fluids, and its building blocks are biodegradable which can be utilised by the body. Furthermore, it can be easily handled, stored and transported [6]. Since its discovery in the early 1990s by Zhang *et al.* during their study on the Z-DNA binding proteins, RADA16-I peptide has been given a significant importance as a scaffold for tissue engineering and as a drug carrier [87, 88].

1.4.2.1 RADA16-I and drug delivery

The foundation of using peptide hydrogels in drug delivery is based on the ability of their injectable forms to self-assemble inside the body and act as vehicles for various drugs and bioactive molecules [2].

Nagai *et al.* reported the release profiles of several dyes (phenol red, bromophenol blue, 8-hydroxypyrene-1, 3, 6-trisulphonic acid sodium salt (3-PSA), 1, 3, 6, 8-pyrenetetrasulphonic- acid tetrasodium salt and Coomassie Brilliant Blue G-250) by using RADA16-I hydrogel as a carrier for drug release formulation. These dyes have different charge densities in spite of their similarities in structure and size. Variant patterns of diffusion from RADA16-I were demonstrated. Two affecting factors were suggested for this difference; the electrostatic interactions between the hydrogel and the dyes, which depends on the amino acid sequence, and the concentration of peptide. The peptide concentration is inversely proportional to the diffusivity of the tested dyes [89].

Gelain *et al.* [90]. also showed that RADA16-I can be exploited in drug delivery applications. The slow and sustained release of three active cytokines (basic fibroblast growth factor BFGF, vascular endothelial growth factor VEGF, brain-derived neurotrophic factor BNDF) from self-assembling RADA16-I scaffolds reported another successful application of this peptide-based hydrogel as a drug carrier.

Liu *et al.* [91] used RADA16-I to deliver the hydrophobic anticancer drug, Paclitaxel. The hydrogel-drug complex formed colloidal suspensions after simple stirring, and showed controlled release behaviour.

Other forms of RADA have also been used as drug delivery devices. A study was carried out by Koutsopoulos *et al.* to investigate the diffusion of functional proteins (lysozyme, trypsin inhibitor, BSA and IgG) from RADA4 hydrogel by utilising fluorescence correlation spectroscopy analysis technique [92]. They reported that the diffusion kinetics depend on the size of proteins. Their results showed that this hydrogelator can be used as a sustained release system for protein-based drugs.

Davis *et al.* demonstrated that RADA-II can be used to deliver insulin-like growth factor 1 (IGF-1) into infarcted cardiac myocytes in rat models, where a biotin-sandwich technique was used to tether the factor to the hydrogel. This approach allowed binding of biotinylated IGF-1 to the self-assembling RADA-II without interfering with the self-assembly [93]. RADA-II provided a sustained release mode of the growth factor to the myocardium. This approach can be used to improve cardiac myocytes therapy.

1.4.2.2 RADA16-I in cell culturing and tissue engineering

Owing to its biomimetic feature and the ability to form stable 3-D structures, RADA16-I has been widely used in many studies as extra-cellular matrix for cell culturing and tissue engineering. Zhang *et al.* reported for the first time, in 1995, that RADA16-I is able to support the attachment of mammalian cells for a long time [37].

In 2000, Holmes *et al.* found that RADA16-I can act as a permissive substrate for neuronal rat cell line PC12 attachment, differentiation and outgrowth [94]. In another study by Semino *et al.*, RADA16-I fostered the expansion and differentiation of rat hepatocyte progenitor stem cells (Lig-8) into hepatocyte-like cells [95].

The same group developed a 3-D environment for neuroprogenitor cells by using RAD16-I as a scaffold. According to their studies, the self-assembling hydrogel can support and enhance the cell migration and tissue growth [96]. Bokhari *et al.* demonstrated the impact of a hybrid hydrogel of RADA16-I and PolyHIPE polymer upon osteoblasts. The combined material provided a permissive microenvironment for the cells where they could keep their osteoblastic phenotype [97].

In a similar study, Horii *et al.* explored the effect of designed RADA16-I with other peptide motifs (ALKRQGRTLYGF, DGRGDSVAYG, and PRGDSGYRGDS) on pre-osteoblasts cell line (MC3T3-E1). The designer peptides promoted osteogenic differentiation and cell proliferation more than RADA16-I scaffold alone [98].

Horii *et al.* carried out a study on pre-osteoblasts to investigate their proliferation. They demonstrated that RADA16-I can be mixed with another peptide RGDA16 to form a new scaffold which enhanced the proliferation of the cells better than the individual peptides [98].

Guo *et al.* reported that self-assembling RADA16-I scaffolds act as a 3-D environment to repair injured spinal cords in rat models. These scaffolds provided bridges for vascular growth and cell migration and differentiation [53].

The compatibility of RADA16-I, pluronic F127 and Matrigel hydrogels with human fetal neural stem cells was studied by Thonhoff *et al.* RADA16-I hydrogel showed lower toxicity, and enhanced the neuronal differentiation of the cells more than the two hydrogels *in vitro* [99].

Kao *et al.* used RADA16-I as a scaffold in preparing synthetic dermis and skin from human fibroblasts and keratinocytes respectively [100].

RADA16-I has also been investigated for therapeutic potential such as wound healing, anticancer activity and nerve repair. Wang *et al*. used RADA16-I to stop bleeding in animal models [101]. They examined the sonication time effect on the peptide self-assembly and its influence on the time required for bleeding control. According to this study, increase of the sonication time results in increase of the time required for bleeding cessation.

In another study by Wen *et al*., the self-assembled RADA16-I was tested to explore its *in vitro* and *in vivo* effect on the growth of malignant pancreatic cells. The results showed that this hydrogelator has a suppressing effect on these cells suggesting a useful application of RADA16-I in pancreatic tumour therapy and research [102].

Moradi *et al.* reported that human fetal Schwann cells can survive in a 3-D RADA16-I scaffold not only *in vitro*, but *in vivo* as well suggesting that this hydrogel is a robust material for repairing spinal cord injuries [103].

Kakiuchi *et al*. examined the differentiation of Human promyelocytic leukaemia cells (HL-60 cells) when cultured in a RADA16-I hydrogel which provided a 3-D microenvironment for the cells. The self-assembling system induced the cells to differentiate into monocytes/macrophages. Also, the intracellular cholesterol increased ten times in the seeded cells in comparison with normally cultured cells [104].

Tokunaga *et al.* found that RADA16-I is a safe and effective biomaterial which can be used to deliver cardiac progenitor cells to a myocardial infarction area in a mouse model. The results suggested that the implantation of cSca-1/ RADA16-I inhibits apoptosis and promotes myocardial regeneration via angiogenesis [105].

1.4.2.3 RADA16-I and mesenchymal stem cells

Mesenchymal stem cells (MSCs) are multipotent cells that have the ability to differentiate into various linages including osteoblasts, adipocytes, chondrocytes, neurons, and myoblasts, (Figure 6) [106]. The therapeutic potential of MSCs in cell-based regenerative medicine and tissue engineering is based on their capability to differentiate in response to the physical changes in their ECM in the absence of chemical treatment [107].

It is becoming increasingly evident that ECM elasticity and nanotopography have impacts upon the differentiation of stem cells [107]. Engler *et al.* showed that ECM stiffness guides the linage differentiation of MSCs. In this work, human MSCs were plated on different polyacrylamide gels to mimic normal environments. The elasticity of these gels was determined by measuring the elastic modulus. MSCs cultured on the soft gels (which mimic brain stiffness) differentiated into neurons, cells on ten times stiffer materials (like muscle elasticity), yield to myoblast-like cells, while on the stiffest matrices osteoblast-similar MSCs were generated [108].

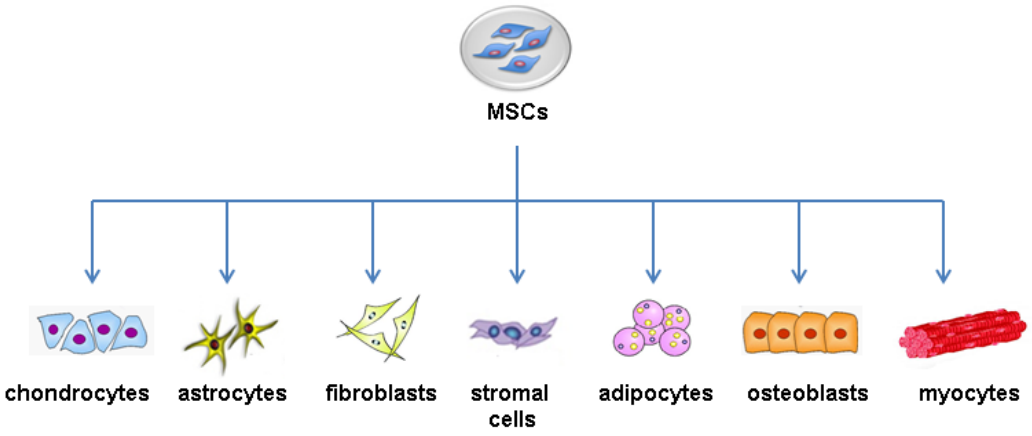

Figure 6 Mesenchymal stem cells differentiation, adapted from [108].

In their article, published in 2007, Dalbey *et al.* demonstrated for the first time that nanotopographies (roughness) of matrices has considerable effect on the mesenchymal differentiation as MSCs were stimulated to produce osteoblasts even in the absence of osteogenic induction media [109].

RADA16-I, as mentioned in 1.4.1, can self-assemble to form nanometre-scale networks composed of β-sheet secondary structures and further to create 3-D scaffolds mimicking the role of the naturally occurring ECM and thus it can support MSCs attachment, growth and differentiation.

In a paper published in 2008, Hamada *et al*. showed that RADA16-I supports the attachment of MSCs isolated from rat bone marrow and encapsulated in the peptide, and induces the osteogenic differentiation *in vitro* in the presence of induction medium (β-glycophospahte, ascorbic acid and dexamethasone). Alkaline phosphatase (ALP) activity and osteocalcin content, which are usually used as biomarkers for bone formation, were higher in the dexamethasone-treated than dexamethasone-untreated cells, and significantly higher than that of the MSCs plated on normal tissue culture plastic without RADA16-I [110].

Erickson *et al.* demonstrated that RADA16-I can promote bovine MSCs to undergo chondrogenesis when the cells are encapsulated in the hydrogel [111].

The *in vivo* ability of RADA16-I hydrogel as a 3-D scaffold for bone regeneration was investigated by Yoshimi *et al.* in 2009. In this study, graft materials, composed of dog MSCs with the peptide hydrogel platelet-rich plasma, were implanted into bone defects in the mandible of a dog. The bone regenerated by RADA16-I /MSCs/ platelet-rich plasma was extremely good, and mature bone was generated [112].

In their work, Matsumoto *et al.* reported that hydroxyapatite ceramics can be incorporated into MSCs/ RADA16-I to form MSCs/ RADA16-I/ hydroxyapatite ceramics composites. These composites enhanced the mechanical properties of the ECM and directed the MSCs toward osteogenesis differentiation [113].

A novel silk/ RADA16-I scaffold was developed by Chen *et al*. Silk-based fibres have good mechanical properties, however, their role as ECM are less effective. In this research, RADA16-I was used to coat a knitted silk in order to provide scaffolds that mimic the 3-D ECM and support the attachment and differentiation of murine bone marrow MSCs. Compared to the uncoated silk, the results showed that the silk/peptide scaffold enhanced the cell proliferation and fibroblastic linage differentiation [114].

The thermal effect on human bone marrow-derived MSCs using RADA16-I as a 3D scaffold *in vitro* was explored by Chen *et al*. in 2013. According to this study, osteogenesis was remarkably improved due to mild heat shock, suggesting the beneficial role of heating approaches in bone regenerative therapy [115].

1.5 Physicochemical characterisation techniques

There is a growing realisation of the need to perform detailed characterisations as hydrogels have become interesting material for biomedical applications. The characterisation of hydrogels is exploring their physical and chemical properties. It is quite challenging as they are highly-soft solvated materials. Since hydrogels are polymers, their physical characteristics are related to the nature of their composite monomers. Additionally, hydrogels contain water, thus, polymer/ water ratio also has impacts on the physical properties [13]. Different means are used to characterise

hydrogels. Structural characteristics can be explored by X-ray diffraction [116] and spectroscopic techniques such as FT-IR [117], CD and NMR [5]. Scanning probe microscopy such as AFM is used to study the surface topography of the self-assembling hydrogels [25]. Viscoelastic properties are quantified by rheometer [118, 119]. Hydrogels are disperse systems. Thus, the molecular size distribution can be measured using multi angle laser light scattering (GPC-MALLS) [120]. Differential scanning calorimetry (DSC) technique is used to investigate the thermodynamic behaviour of hydrogels and quantify the free and bound water amounts [26]. The purity of polymeric hydrogels and the concentrations of their monomers can be quantified using HPLC [121].

However, in this section, only the techniques that are used in this study will be discussed.

1.5.1 Fourier transform infra-red (FT-IR) spectroscopy

The infra-red region (2,500-20,000 nm or 400-4,000 cm^{-1}) of the electromagnetic radiation absorbed by the bonds of molecules can be used as a qualitative fingerprint check to confirm the chemical structures of materials. The absorbed radiation by bonds, at specific wavelengths, makes them stretch or bend, thus, those wavelengths (wavenumber) are characteristic of the absorbing bonds [122]. In peptide-based hydrogels, FT-IR is used to assign the peak of the amide I region (1,700-1,600 cm^{-1}). This region is more informative for secondary structures due to the stretching vibration of the carbonyl bond C═O. Structural changes in peptide hydrogels cause alterations in the wavelengths at which absorption happens [123]. Table 1 shows the FT-IR assignments of amide I of secondary configurations in polypeptides and proteins.

Table 1 Amide characteristic IR bands of peptide [124]

Secondary Structure	**IR region in H_2O (cm^{-1})**	**IR region in D_2O (cm^{-1})**
α-helix	1648-1657	1642-1660
β-sheet	1623-1641	1615-1638
β-sheet	1674-1695	1672-1694
Turns	1662-1686	1653-1691
Random	1642-1657	1639-1654

Other amide bands (Table 2) are less practical since they are complex due to hydrogen bonding and side chains.

Table 2 IR bands of amide I of peptide secondary structures [123]

Designation	Frequency (cm^{-1})	Description
Amide A	3300	NH stretching
Amide B	3100	NH stretching
Amide I	1600−1690	C=O stretching
Amide II	1480-1575	CN stretching, NH bending
Amide III	1229−1301	CN stretching, NH bending
Amide IV	625−767	OCN bending
Amide V	640−800	Out-of-plane NH bending
Amide VI	537−606	Out-of-plane C=O bending

1.5.2 Circular dichroism (CD) spectroscopy

The circular dichroism phenomenon was first discovered by three French scientists, Augustin-Jean Fresnel, Jean-Baptiste Biot and Aimé Cotton, in the nineteenth century. This spectroscopic technique depends upon the deferential absorption of the left and right circularly-polarised components of the plane-polarised light. It is characteristic for chiral molecules which are optically active *i.e.* containing chromophores. If a sample absorbs one component more than the other, resultant (combined) light would be elliptically polarised [125]. The chirality is either intrinsic or extrinsic. Intrinsic chirality is exhibited by materials containing chiral centre(s) in their chemical structures, while extrinsic chirality occurs when molecules are present in a chiral environment [126]. Although many polypeptides and proteins are composed of amino acids containing chiral centres, the peptide (amide) bonds are the main absorbing groups in the far UV region (between 180 and 240 nm) and thus give information about the secondary α-helix and β-sheet structures. In the near UV (260 to 320 nm), which corresponds to aromatic amino acid side chain and/or disulphide bond absorption, the spectrum reflects the tertiary structure [127]. Table 3 shows the amide (peptide bond) transitions in the near UV region.

Table 3 Peptide bond transitions in the near UV region [128]

Transition type	Wavelength (nm)
$n \rightarrow \pi^*$	210
$\pi \rightarrow \pi^*$	190
$n \rightarrow \pi^*$	165
$\pi \rightarrow \pi^*$	125

The CD spectra of α-helical peptides display two negative bands near 208 nm and near 222 nm, and a strong positive band near 192 nm, while in β-sheet peptides, a positive band between 194 and 200 nm and a negative band near 215 nm are observed [125]. CD is a valuable tool that has been used for the structure content conformation of proteins and peptides and studying their stability and behaviour in different experimental conditions like pH, temperature, presence of ligands and ionic strength [129]. Figure 7 illustrates the CD spectra of myoglobin which contains approximately 72 % α-helix [128], and RADA16-I which is mainly composed of β-sheets.

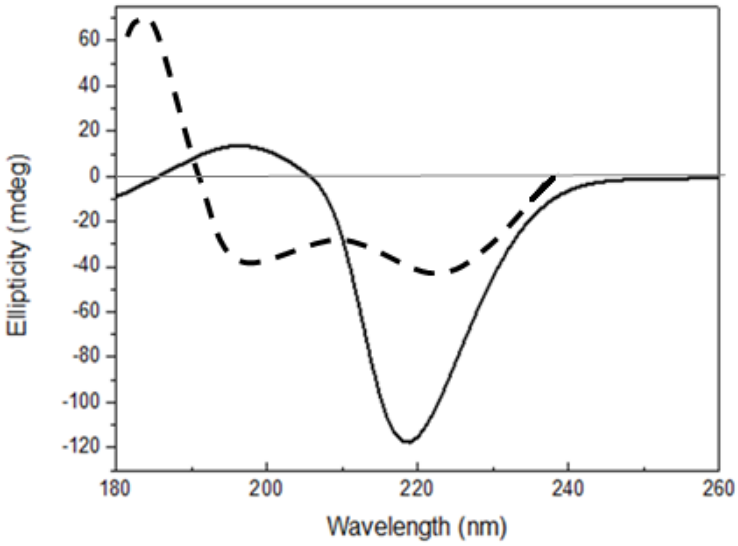

Figure 7 CD spectra of RADA16-I (solid line, β-sheet) and myoglobin (dash line, α-helix)

1.5.3 Atomic force microscopy (AFM)

Scanning probe microscopy (SPM) is a group of imaging techniques capturing images of the surfaces of materials [130]. Atomic force microscopy (Figure 8) is the most common type of SPM. It can be applied to almost any sample such as polymers, metals, cells, bacteria. [131]. It can be used in a vacuum, air or liquid. Most interestingly, it is like a surface profiler that not only gives high-resolution images of a sample's surface, but also provides detailed quantitative information about the topographic and mechanical features at the nanoscale such as length, thickness, rigidity and roughness of fibres [132]. In AFM, samples do not need to be stained or coated with metals [133]. Since its invention by the Nobel-Prize winners, Gerd Binnig and Heinrich Rohrer in the1980s, AFM has become the principal technique used in the nanoscale characterisation of materials [131]. AFM uses a probe (tip and cantilever) that moves across a surface in a raster (vertical and zig-zag) pattern. The tip of the probe is the part that actually interacts (feels) with the surface

of the sample. A laser is used to measure the topography by measuring its deflection from the cantilever and then sent to a feedback programme to be analysed. An image is created by plotting its horizontal and vertical movements as the tip scans across the surface [134]. Depending on the application, AFM can be operated in several scanning modes. **Contact mode**: the probe tip is in physical contact with the sample where the force is kept constant. In this mode the cantilever deflection is measured to track the surface morphology using a feedback loop [135].

Non-contact mode: the probe tip oscillates in resonance frequency with amplitude of several tens of nm. In this mode the oscillation amplitude of the cantilever is measured to track the surface morphology by a feedback loop [134]. **Tapping (intermediate contact) mode (TMAFM)**: This mode was developed (patented by Digital Instruments, now Bruker in 1993 [136]) to solve some of the problems of both the contact and intermittent contact modes. In this mode, the cantilever is excited to oscillate at its mechanical resonance frequency. The tip intermittently comes in contact with the sample resulting in change in the oscillation amplitude which can be exploited to discover the surface topography of materials, and thus can provide much better imaging results, especially in liquid environments [137].

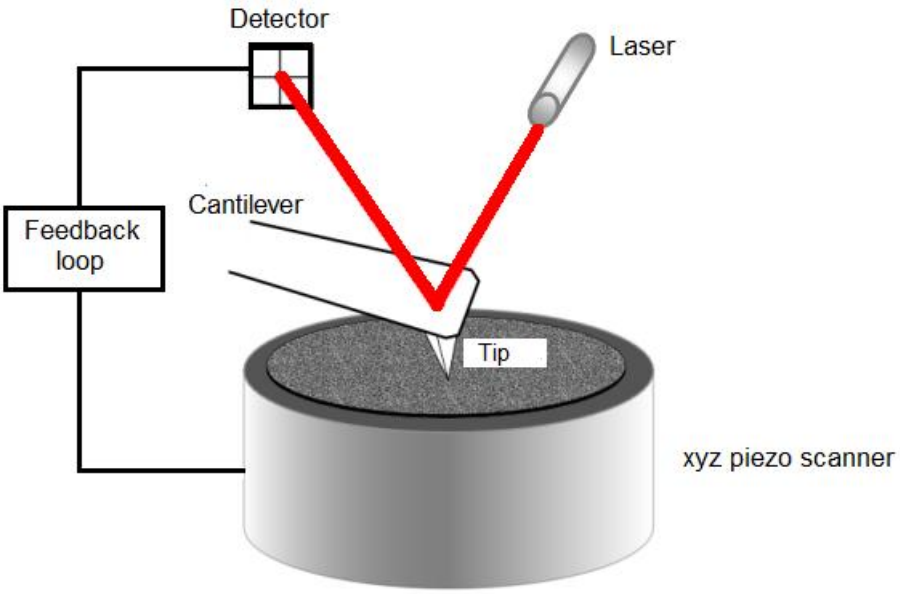

Figure 8 A simplified diagram of AFM.

The high-quality topographic and phase imaging information created by this technology have made it the main scanning mode over the last twenty years. However, it is impractical in terms of generating precise quantitative mechanical data as the oscillating operation of the probe works as a filter for the forces experienced by it [132].

Many methods have been developed in order to tackle this drawback. **Peak Force-Quantitative Nanomechanical Mapping (PF-QNM)**, invented by Veeco, is one of the newest and most powerful techniques that provides such flexibility for researchers to characterise the surface of materials quantitatively at the nanoscale level [138]. As PF-QNM is used in this project, it will be discussed in detail.

Peak force tapping (PFT) method is the heart of PF-QNM. PFT is similar to TMAFM in the contacting behaviour where the probe intermittently touches the surface for a short period. In PFT, the peak force (maximum on the tip) is precisely kept constant which

differs from TMAFM where the probe vibration amplitude is controlled by the feedback loop.

Figure 9 illustrates the "Force Curve", the basic concept of PF-QNM. At point **A**, the force on the tip is almost zero as the cantilever is far away from the sample. When the tip approaches the sample surface, forces (like van der Waals and capillary interactions) attract the cantilever to the surface (point **B**). The distance between the surface and the cantilever decreases till it reaches its lowest position (point **C**). At point C, the peak force appears. The feedback loop keeps this force at a constant level. A reverse phenomenon happens when the cantilever moves away from the surface due to the repulsive forces, and the force applied on the tip declines until point **D** which reflects the adhesion. At point **E**, the force is negligible or zero again as the space between the tip and the surface is at its maximum [139].

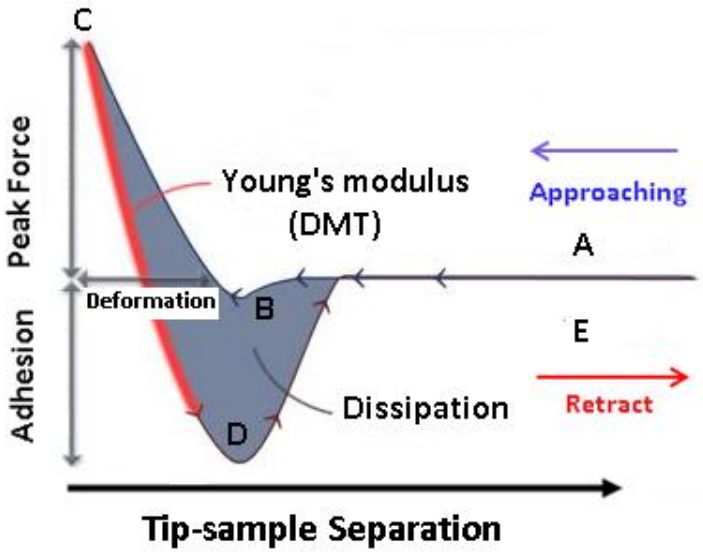

Figure 9 A force-separation curve obtained using AFM nanomechanical mapping. DMT is the Derjaguin–Muller–Toporov model which is used to obtain the elastic modulus, adapted from [139]

The PF-QNM relies on the ability to obtain and separately analyse the force curves acquired from the individual taps that occurs due to the instantaneous force applied on the tip when the probe moves across the surface [138]. Mechanical properties that are included in the force curves, such as elastic (Young's) modulus, adhesion and deformation, are measured separately and precisely [132].

In hydrogels, different AFM modes can be applied to characterise a number of properties such as the shape and geometry of the formed structures, conductivity, adhesion, and the Young's modulus [140].

1.6 Aims and objectives

There are three main aims for this project. **The first aim** was to investigate the use of ionic salts (Hofmeister series), such as sodium sulphate and sodium iodide, to trigger the self-assembly of RADA16-I hydrogel. **The second aim** was to explore the use of the salt induced-self-assembled hydrogels for drug delivery, with the primary consideration for the release of quinine. Quinine is a hydrophobic drug, and the solubility of hydrophobic drugs in the aqueous media is a major problem in the pharmaceutical industry. **The third aim** was to study the impact of the hydrogels upon the adipogenic and osteogenic differentiation of murine C3H10T1/2 stem cells.

The first phase was to characterise the prepared hydrogels and examine their stability under physiological conditions to understand how the molecular structure of the peptide is affected by different salts. This was performed using three specialised techniques; CD, FT-IR and AFM in order to explore the change in the β-structure of RADA16-I due to the interaction with the anions. The second phase involved investigating the release of quinine from the hydrogels. This was done using UV-spectroscopy to measure the concentrations of the drug released from the systems. Finally, the behaviour of the C3H10T1/2 stem cells seeded on the 2-D hydrogels was investigated in addition to the cytotoxicity of sulphate and iodide sodium. Since the cells failed to adhere to the hydrogels, fibronectin was used to induce cell attachment and spreading.

Chapter two: Materials and methods

2.1 Materials

The following materials were purchased from Sigma-Aldrich (UK): sodium citrate (≥ 98.8%), sodium phosphate monobasic (≥ 99.0%), sodium chloride (≥ 99.5%), sodium nitrate (≥ 99.0%), sodium perchlorate(≥ 98.0%) , sodium thiocyanate (≥ 98.0%), sodium iodide (≥ 99.5%), quinine (≥ 98.0%), phosphate buffer saline tablets, paraformaldehyde (95.0%), fibronectin sterile solution (0.1%), 3-isobutyl-1-methylxanthine (≥ 99.0%), dexamethasone (≥ 97.0%), Oil Red O, isopropanol solution, L-Ascorbic acid (≥ 99.0%), β-Glycerophosphate disodium salt hydrate (≥ 99.0%), retinoic acid (≥ 98.0%), boric acid (≥ 99.5%), P-nitrophenol (≥ 99.5%), Triton X-100 solution , magnesium chloride (≥ 98.0%), formalin solution (≥ 36.0%), silver nitrate (≥ 99.0%) and pyrogallol (≥ 98.0%). RADA16-I hydrogel (PuraMatrix, CH3CO–NH–(Arg-Ala-Asp-Ala) $_4$–CONH2, 1% w/v) was purchased from BD Bioscience (MA, USA). Murine mesenchymal (C3H10T1/2) stem cells were purchased from ATCC, Manassas, VA, USA. Recombinant BMP4 was purchased from R&D Systems (USA). The following cell culture materials were purchased from Life Technologies (UK): Dulbecco's Modified Eagle Medium (DMEM), fetal bovine serum, (penicillin/ streptomycin), MTT ((3-(4, 5-dimethylthiazol-2-yl)-2, 5-diphenyltetrazolium bromide), Alamar blue and human recombinant insulin.

2.2 Analysis Instruments

Circular dichroism measurements were performed by Chirascan™-plus spectrophotometer (Applied Photophysics Ltd, UK).

FT-IR spectra were recorded on a Nicolet iS10 Smart FT-IR spectrophotometer (Thermo Scientific Inc., USA).

AFM images were obtained by scanning the mica surface (G250-2 mica sheets, Agar Scientific Ltd., Essex, UK) using a scanning probe microscope (Bruker MultiMode with a NanoScope V Controller 8; and Bruker Nanoscope analysis software version 1.40, Bruker UK Ltd, Coventry, UK), operating using the new mode PeakForce QNM. The AFM measurements were obtained using sharp silicon probes (ScanAsyst-air, Bruker UK Ltd, Coventry, UK)

2.3 Methods

2.3.1 RADA preparation and gel formation

RADA16-I samples were prepared by adding 2.5 µL of 100, 300, 600 and 900 mM of each of sulphate, citrate, phosphate monobasic, chloride, nitrate, perchlorate, thiocyanate and iodide sodium salts to 100 µL of RADA16-I in the presence of 2.5 µL of phosphate buffer. The samples were then left overnight at 4°C before carrying out the experiments.

The stability test samples were prepared by adding a 2.5 µl of 600 mM of sulphate and iodide sodium salts to a 100 µl of RADA16-I in the presence of a 2.5 µl of phosphate buffer. A control sample was prepared without adding salts. Samples were left at 37°C for 14 days. The samples were washed every 3 days with 3×400 µL of PBS with an interval of 10 minutes. The experiment was repeated three times.

2.3.2 Samples preparation in the presence of paraformaldehyde

A 4% (w/v) PFA solution was prepared by dissolving the PFA powder in PBS. RADA16-I samples were prepared by adding a 2.5 µl of 600 mM of sulphate and iodide sodium salts to a 50 µl of RADA16-I in the presence of a 50 µl of PFA.

Another set of samples was prepared, for stability test, by the same method and left at 37°C for 14 days. They were washed every 3 days with 3×400 µL of PBS with an interval of 10 minutes. The experiment was repeated three times.

2.3.3 Circular dichroism

CD measurements were performed using a 0.1 mm pathlength quartz cuvette. The supported parameters: λ = 180–260 nm, λ *(*bandwidth*)* = 1 nm, time constant = 1 s, using 3-times scans for average at 25 °C. In order to investigate the effect of salts on secondary structures and self-assembling nanofiber formation of RADA16-I, a software programme "CDNN", CD spectra deconvolution software, was applied to estimate secondary-structure components.

For the stability, the CD was run for the supernatants after the third wash on days 1, 5, 10 and 15, and for the gels on day 15.

2.3.4 Fourier transform infrared (FT-IR) spectroscopy

The spectra were taken in the region 4000 and 500 cm^{-1} over 128 scans at a resolution of 4 cm^{-1} and an interval of 1 cm^{-1}. Here the region 1740 and 1560 cm^{-1} was shown, since

that region shows the β-sheet structure, which was used to validate the CD results. In order to correct the background effect, the spectrum of phosphate buffer solution was subtracted from the spectrum of each hydrogel sample.

2.3.5 Atomic force microscopy

5 µl sample was deposited onto a freshly cleaved mica surface (1.5 cm x 1.5 cm) and left on the mica for 45 min air-dried, and images were acquired immediately at room temperature. The images were obtained by scanning the mica surface in air under-ambient conditions using the AFM operated in the new mode PeakForce QNM. The AFM measurements were obtained using ScanAsyst-air probes, for which the spring constant (0.58 N/m; nominal 0.4 N/m) and deflection sensitivity had been calibrated, but not the tip radius (the nominal value used was 2 nm). AFM images were collected from two different freshly prepared samples and at random spot surface sampling (at least five areas per sample).

2.3.6 Drug release

Quinine solution at a concentration of 0.5 mg ml^{-1} was prepared by dissolving quinine powder in Milli-Q water. RADA16-I hydrogel and RADA16-I with 600 mM sulphate and iodide sodium salts were prepared in 1 ml eppendorf tubes as described in 2.2.1. The hydrogels incorporating quinine were prepared by adding 4 µl of quinine solution into the tubes, followed by vortexing for 30 s, and then the samples were left for 20 minutes at 4°C before taking the release measurements. The drug release was carried out by taking

samples of 400 µl from the supernatant (without disturbing the hydrogels) and replaced with the same volume of PBS solution. The release experiments were performed at 37 °C, for a period of 3 days, where the supernatant drugs concentration was measured at 15 min, 30 min, 1, 2, 3, 4, 24, 48 and 72 h. To satisfy the perfect-sink conditions which allow for the determination of the diffusion parameters, the supernatant was replaced with fresh PBS at 37 °C at each time point. The concentration of the drug molecules inside the hydrogel and in the supernatant was determined by UV-Vis spectrophotometer. The concentration of the drug molecules released from the hydrogel was determined using a calibration curve of the pure drug molecules in PBS solution at the wavelength showing the maximum absorbance.

2.3.7 Mesenchymal stem cells (MSCs) culture and differentiation

2.3.7.1 Growth curve

Murine mesenchymal (C3H10T1/2) stem cells were cultured in a growth medium composed of Dulbecco's Modified Eagle Medium, DMEM, 10% (v/v) fetal bovine serum and 1% v/v (penicillin/ streptomycin). The cells were subcultured when they reached 80 % confluence. The cells were seeded in three densities (1000, 5000 and 1000 cell/cm^2) on 96-well plates, left in a humidified atmosphere (37˚C, 5% CO_2) for one day. The proliferation of the cells was measured using a MTT ((3-(4, 5-dimethylthiazol-2-yl)-2,5-diphenyltetrazolium bromide) proliferation assay. The working reagent (5 mg ml^{-1}) was prepared by dissolving the MTT in PBS. The solution was then sterilised using a 0.22 µm filter, and stored at 4 ˚C in the dark. On day two, 20 µl of the (5 $mg.ml^{-1}$) MTT solution

was added to each well. The plates were incubated for 5 hours at 37 ˚C. The medium was removed and 120 µl of dimethyl sulphoxide (DMSO) was added to each well, and the plates were incubated at 37 ˚C for 10 minutes. A 100 µl from each well was transferred to a new 96-well plate, and the absorbance was measured at 570 nm. The blank absorbance values (DMSO) were subtracted from the values of the experimental data (cells) to exclude the effect of the solvent. The MTT assay measurements were obtained on days 1, 2, 3, 4 and 7.

2.3.7.2 Adipogenic differentiation

The cells were seeded on 24 and 96-well plates at a density of 5000 cell.cm^{-2}, and left to grow for two days in a humidified atmosphere (at 37˚C, 5% CO_2). On day 3, the growth medium was replaced by a medium supplemented with 50 ng.ml^{-1} of recombinant BMP4 which was left for 2 days. After two days, the cells were grown using an adipogenic induction cocktail (10 µg.ml^{-1} insulin, 1 µM dexamethasone and 0.5 mM methylisobutylxanthine), for 2 days and kept with adipogenic maintenance media (10 µg/ml insulin) for an additional 10 days with media changed every 2 days. The cells in the 96-wellplate were maintained as a control without adding the induction medium. On day 14, the cells in the wells were fixed with 10% formalin for 60 min at 5 ˚C and stained with ~ 50 µl of for 30 minutes. The wells were washed three times with PBS. The dye was extracted with isopropanol. Blank (without cells) wells were stained and manipulated in the same methods. The blank absorbance values were subtracted from the values of the experimental data (cells) to exclude the retained stain by the wells' walls. The stained Oil Red O was quantified by measuring the absorbance at 540 nm.

2.3.7.3 Osteogenic differentiation

The cells were seeded at a density of 5000 cell.cm^{-2}, and left to grow for two days in a humidified atmosphere at 37 ˚C and 5% CO_2. The osteogenic induction cocktail was added on day 3. An induction medium containing 0.05 mM ascorbic acid, 10 mM β-glycerophosphate, 10^{-5} mM dexamethasone, and 1 µM retinoic acid was used. Each 96-well plate was divided into two halves one for the osteogenic induction and the second was treated as a control. The induction media were changed every 3 days. On day 21, matrix mineralisation was visualised using a Von Kossa staining method [135]. Protein quantification was carried out using a Thermo Scientific Micro BCA Kit.

2.3.7.4 The cytotoxicity of RADA16-I alone and with sodium sulphate and sodium iodide salts on the C3H10T1/2 cells

600 mM salt solutions were prepared and sterilised using a 0.22 µm filter. RADA16-I samples were prepared by adding 2.5 µl of 600 mM of sulphate and iodide sodium salts to a 100 µl of RADA16-I in the presence of a 2.5 µl of phosphate buffer. Control samples were prepared without adding salts. The samples were sonicated for 30 minutes then plated in 96-well plates (50 µl per well) and left overnight in the fridge.

The plates were divided into two halves where a 50 µl of 5% (w/v) paraformaldehyde (PFA) solution was added on the gels of the wells of one half and kept for 20 minutes, while the second half remained without PFA.

Before adding the cells, the gels were washed over a period of 90 minutes with PBS once and medium twice. The cells were plated on the gels with a density of 5000 cell.cm^{-2}. The proliferation of the cells was measured using an Alamar blue proliferation assay.

2.3.7.5 C3H10T1/2 cell adhesion

RADA16-I gel (without salts) samples were prepared as mentioned above. 50 µl of fibronectin solution (1 mg.ml^{-1}, 0.1 mg.ml^{-1}, 0.01 mg.ml^{-1} and 0.001 mg.ml^{-1}) was added on top of the gels for 60 min, rinsed with cell culture media for 5 min, aspirated, and then the cells were added to the top of the gels. Alamar blue proliferation assay was carried out after 24 h of incubation.

2.3.7.6 Salt cytotoxicity

600 mM sulphate and iodide salt solutions (stock solutions) were prepared and sterilised using a 0.22 µm filter. Two solutions for each salt were prepared; a 500 µl of the stock solution was added to 9.5 ml medium (solution I), and 1ml of solution I was added to 9 ml medium (solution II).

The cells were seeded on two 96-well plates (one for each salt) at a density of 5000 cell.cm^{-2} and left to grow for one day in the incubator (at 37 ˚C and 5% CO_2). The solutions I and II were added to the cells in the following concentration order; 0, 0.3, 0.75, 1.5, 3, 7.5, 15, 21, 28.5, and 30 mM.

The cells were left with the salts for 72 h in the incubator. The MTT assay (at 570 nm) was carried out on the third day.

2.3.7.7 Cytotoxicity of the hydrogels in the presence of sulphate and sodium salts and fibronectin

Samples were prepared as described in 2.2.6.4 with two modifications. PFA was washed with a 0.3 M glycine (in PBS) solution. Secondly, a 0.01 M of fibronectin (FN) solution (50 µl per well) was added. The proliferation of the cells was measured using an Alamar blue proliferation assay.

2.3.7.8 Cytotoxicity in the presence of the hydrogels and different concentrations of sulphate and sodium salts

Samples were prepared as described in 2.2.6.4. This time, different sulphate and iodide sodium salt (10, 100, 300 and 600 mM) solutions were used. Alamar blue proliferation assay was performed on the seventh day.

Chapter three: Results and discussion

3.1 Characterisation of hydrogels

This chapter represents the results obtained from several laboratory techniques used to characterise the physical properties of RADA16-I alone and in the presence of different concentrations of sodium salts. In order to examine the effect of the salts on the hydrogel, four concentrations were used, 100 mM, 300 mM, 600 mM and 900 mM. The impact of the ions and concentrations on gelation was tested using circular dichroism (CD), Fourier transform infrared spectroscopy (FT-IR) and atomic force microscopy (AFM).

3.1.1 Circular dichroism (CD)

The physical properties of RADA16-I hydrogel is affected by the type and concentration of ions. The CD measurement (Figure 10) shows a typical β-sheet structure of RADA16-I with a minimum ellipticity at ~217 nm and a maximum ellipticity at ~196 nm [6, 7].

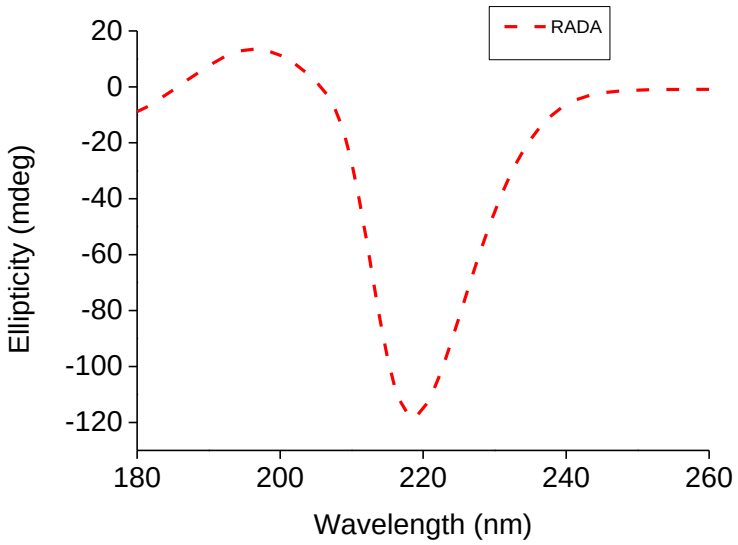

Figure 10 CD spectra of RADA16-I which adopted typical β-sheet structure spectrum.

Figures 11, 12, 13 and 14 illustrate the CD spectra of RADA16-I in the presence of the salts. In the presence of the first concentration (100 mM), the change in the gel's structure did not change significantly. With increasing concentration, RADA16-I secondary structures changed according to the added salts. It can be seen from Figures 13 and 14 that kosmotropic (citrate, phosphate and chloride) ions did not affect the chirality of the self-assembled hydrogels. While with chaotropes (nitrate, iodide, perchlorate and thiocyanate), the CD signals reduced in terms of peaks intensities (molar ellipticity) and positions (red shift) explaining the disrupting effect of these ions on the β-sheet structure of the peptide. Interestingly, at the concentrations 600 and 900 mM, RADA16-I with sodium sulphate formed a viscous hydrogel which was difficult to be measured by CD due to formation of spots when they are applied on the cuvettes. This is due to the strong salting-out effect of the sulphate ion on the peptide [142]. Concentrations 600 and 900 mM had the strongest effect on the gel.

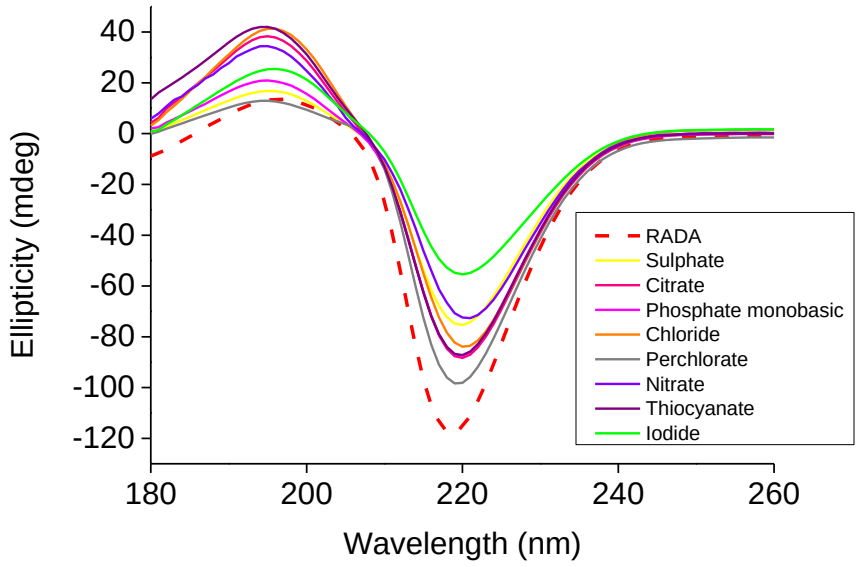

Figure 11 CD spectra of RADA16-I in the presence of different sodium salts at a concentration of 100 mM

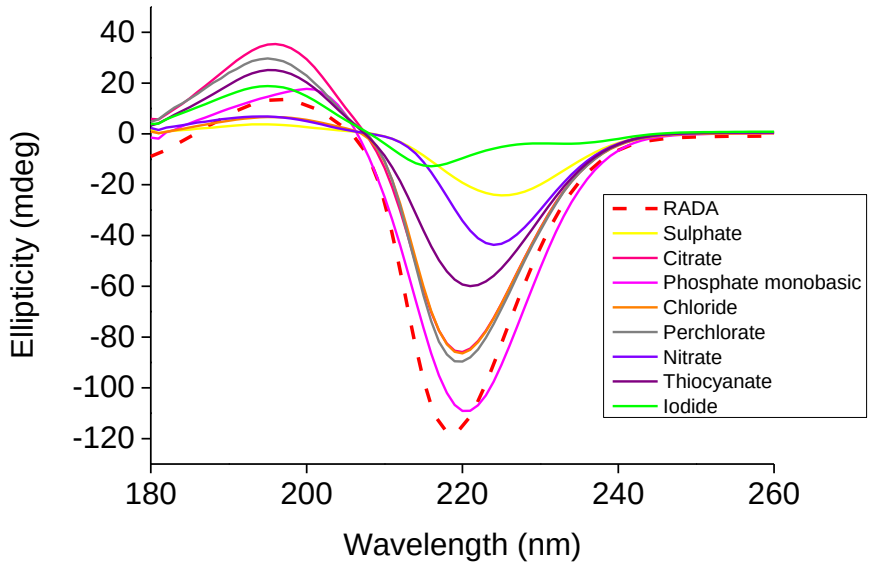

Figure 12 CD spectra of RADA16-I in the presence of different sodium salts at a concentration of 300 mM

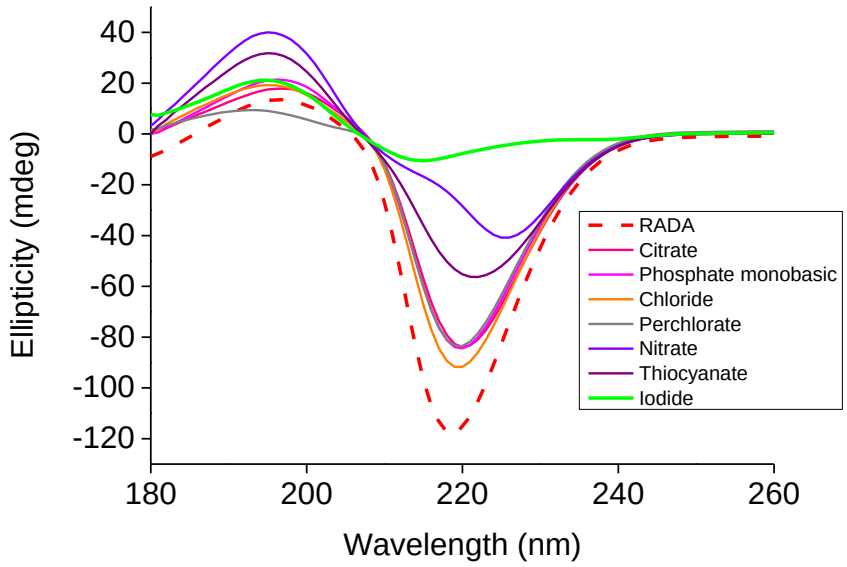

Figure 13 CD spectra of RADA16-I in the presence of different sodium salts at a concentration of 600 mM

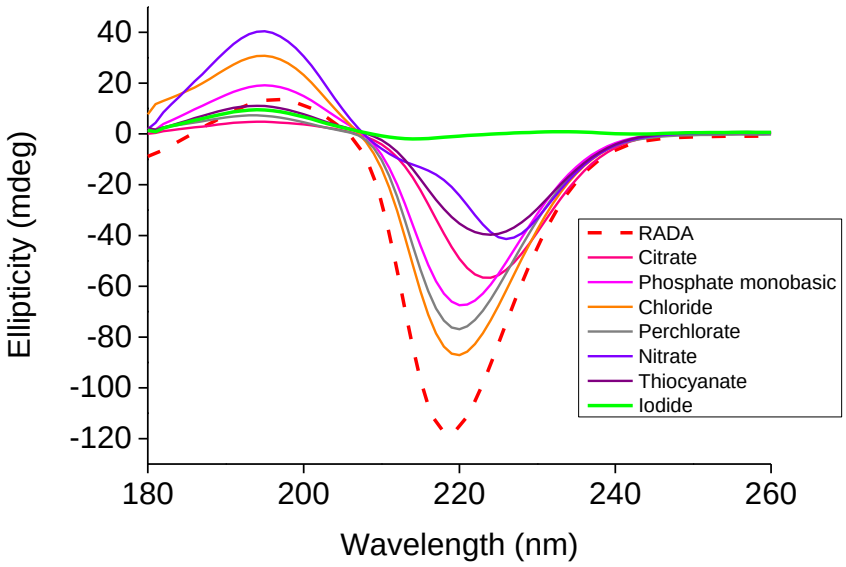

Figure 14 CD spectra of RADA16-I in the presence of different sodium salts at a concentration of 900 mM

Using high salt concentrations has a severe effect on cells [143]. Therefore, it was important to use the minimum effective concentration in order to minimise the cytotoxic effect of the salts on the cells which is dose dependant. Therefore, concentration 600 mM was selected to be investigated further.

CDNN was used to estimate the change in the secondary-structure components. Table 4 shows the effect of the different ions on the β- sheets. The different percentages give additional evidence on the change in the structure due to the effect of the salts. CD results (Figure 13) showed that RADA16-I in presence of 600 mM of chloride, phosphate monobasic, citrate, perchlorate, thiocyanate, nitrate and iodide ions was able to exhibit its β-sheet structure, which can be evidenced by 35.4% to 41.3% β-sheet, according to CDNN software analysis (Table 4). However, the β-sheet content is higher in the presence of kosmotropic ions than chaotropic ions.

Table 4 Estimated structure fractions (%) of RADA16-I in the presence of different sodium salts using CDNN software

Item	α-helix	Antiparallel β-sheet	Parallel β-sheet	β-turn	Random coil
RADA16-I	17.8	35.6	14.1	20.8	44.3
With Chloride	19.4	27.3	14	19.7	46.2
With Phosphate monobasic	20	27.2	13.3	19.7	44
With Citrate	20	26.1	13.6	19.6	45.4
With Perchlorate	20.3	25.4	13.4	19.5	44.8
With Thiocyanate	20.5	25.1	13.3	19.4	44.7
With Nitrate	20.8	24.5	13.2	19.4	44.3
With Iodide	21.7	22.8	12.6	19.2	42.8

3.1.2 Fourier transform infrared spectroscopy (FT-IR)

FT-IR can be used to examine the changes in the amide I region due to the interactions between the hydrogels and the salts. In Figure 15, FT-IR spectra of RADA16-I with the 600 mM salts are illustrated. They are rather similar and show maxima between 1615 and 1619 cm^{-1}, characteristic of the β- sheets in the amide-I region [11]. The small variations of the spectra in this region suggest that RADA16-I has different ordered structures in the presence of the salts.

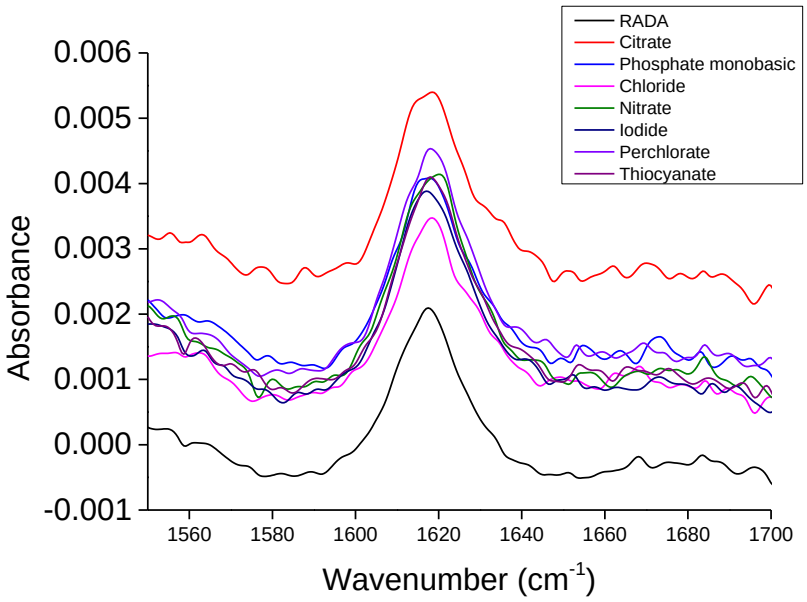

Figure 15 FT-IR spectra of RADA16-I hydrogels in presence of 600 mM sodium salts showing the formation of ß sheets in the amide-I region

Second-derivative peak analysis was carried out on the IR spectra to determine the underlying peaks in the amide-I region. Figure 16 shows the differences between the different gels in terms of the number of the underlying peaks and their positions.

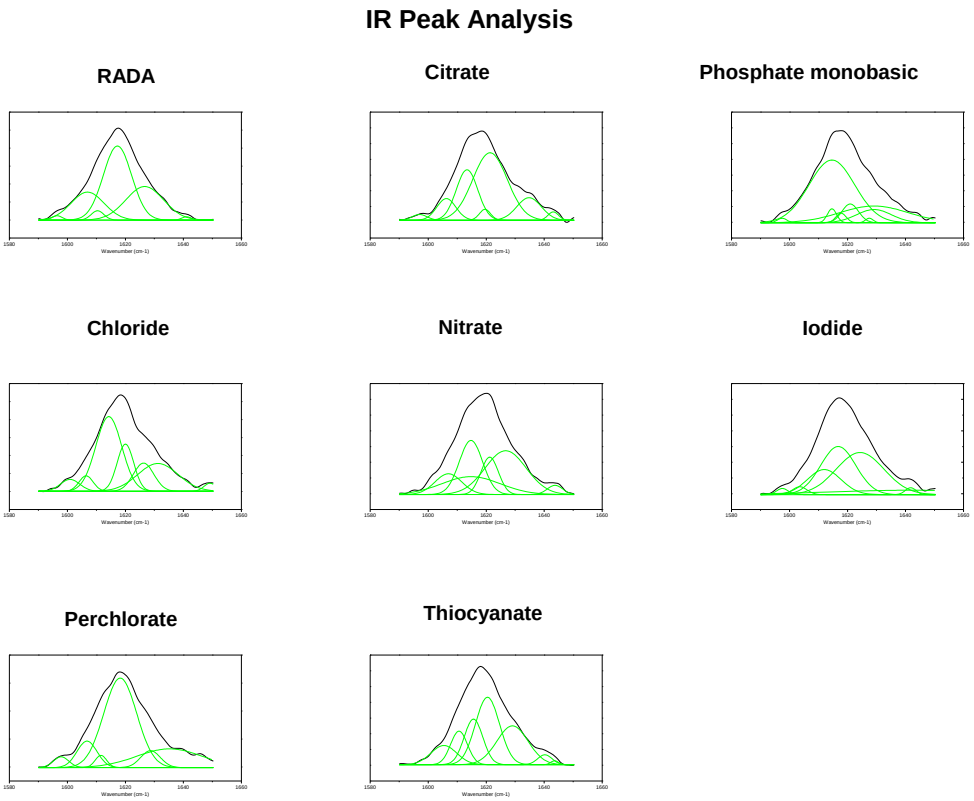

Figure 16 Peak analysis of the IR spectra. Green lines represent peak numbers and positions calculated by second derivative method (OriginPro9.0 software).

The FT-IR and CD results suggest that different salts have different impacts on the secondary structures.

3.1.3 Atomic force microscopy

In order to provide a further insight into the morphology of the hydrogels at the nanoscale level, AFM was performed on RADA16-I in the absence of the salts, and in the presence of sodium sulphate and sodium iodide. Examples of typical AFM images are presented in

Fig. 17 which reveal significant differences. Table 5 summarises some parameters such as diameter (D), surface roughness (Ra) and Young's modulus.

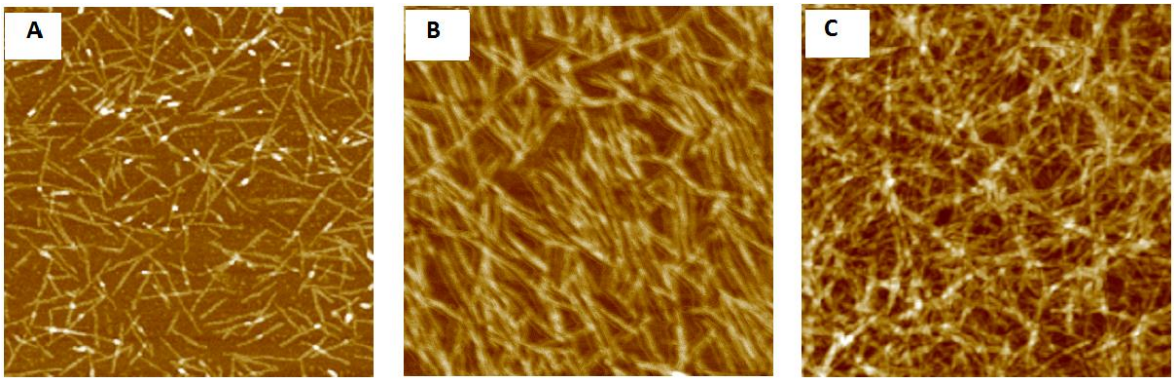

Figure 17 Typical AFM images of the RADA16-I (A) in the presence of sodium sulphate (B) and sodium iodide (C). Scale 1μm ✕ 1μm

Table 5 Image analysis of RADA16-I hydrogel in presence of salts

Hydrogel	D/ nm	Ra/ nm	Young's Modulus/ GPa
RADA16-I	23.4 ± 2.1	0.5 ± 0.1	47.5 ± 3.0
With sulphate	40.8 ± 3.7	1.4 ± 0.1	36.6 ± 0.9
With iodide	32.8 ± 2.2	1.3 ± 0.3	25.7 ± 1.5

RADA16-I hydrogel showed thin nanofibers (23.4 ± 2.1 nm in diameter), 0.5±0.1 nm surface roughness and Young's modulus of 36.6 ± 0.9 GPa. Nanofibers formed in the presence of sodium sulphate showed a thick morphology with diameters of 40.8 ± 3.7 nm, surface roughness of 1.4 ± 0.1 nm and Young's modulus of 36.6 ± 0.9 GPa. In contrast, in the presence of sodium iodide, dense fibres with diameters of 32.8 ± 2.2 nm, surface roughness of 1.3 ± 0.3 nm and Young's modulus of 25.7 ± 1.5 GPa were observed. It can be concluded that sulphate and iodide ions have different effects on the self-assembly of the hydrogel.

RADA16-I hydrogel, as an ionic self-complementary peptide, can assemble in water due to a combination of hydrophobic and hydrogen interactions [71]. Alanines are responsible for forming the hydrophobic interactions in the aqueous medium while the hydrogen-bonding interactions result from the amide groups [69]. The results discussed here show that ionic salts significantly influence the nanostructure of RADA16-I. They also suggest that sulphate (kosmotropic) induces hydrophobic interactions in addition to hydrogen bonding. These contributions seem weaker in the presence of chaotropic (iodide) ions [121].

3.2 Stability of RADA16-I under the physiological conditions

Based on a theory proposed in the literature, the self-assembly of peptides should occur at a pH around 7 where van der Waals attractions overcome intermolecular electrical repulsive forces according to the Derjaguin–Landau–Verwey–Overbeek hypothesis [149, 150]. Nevertheless, only a few numbers of peptides can exhibit stable β-structures in aqueous media without using stabiliser(s) [151]. Many reports claimed that RADA16-I can form stable secondary structures in the physiological conditions [6, 10, and 11].

A two week study was conducted in order to investigate the stability of RADA16-I hydrogels (RADA16-I, RADA16-I with sodium sulphate and RADA16-I with sodium iodide) at the neutral pH and 37˚C.

The CD measurements (Figure 18) illustrate that the *β*-sheet structures were impaired due to the effect of the pH even in the presence of sulphate and iodide ions in comparison to the peptide at acidic pH which showed a typical β-sheet structure with a minimum

ellipticity at 219 nm and a maximum ellipticity at 197 nm at room temperature without washing with PBS, Figure 12.

The AFM images (Figure 19) confirmed the CD findings. Typical highly dense nanofibers were obtained with RADA16-I sample at room temperature without PBS washing (Figure 17 (A)). When the samples were washed with PBS, the gels formed irregular aggregates, Figure 19 (A), (B), and (C), rather than nanofibres. It is obvious that the self-assembly was disrupted at the experimental conditions.

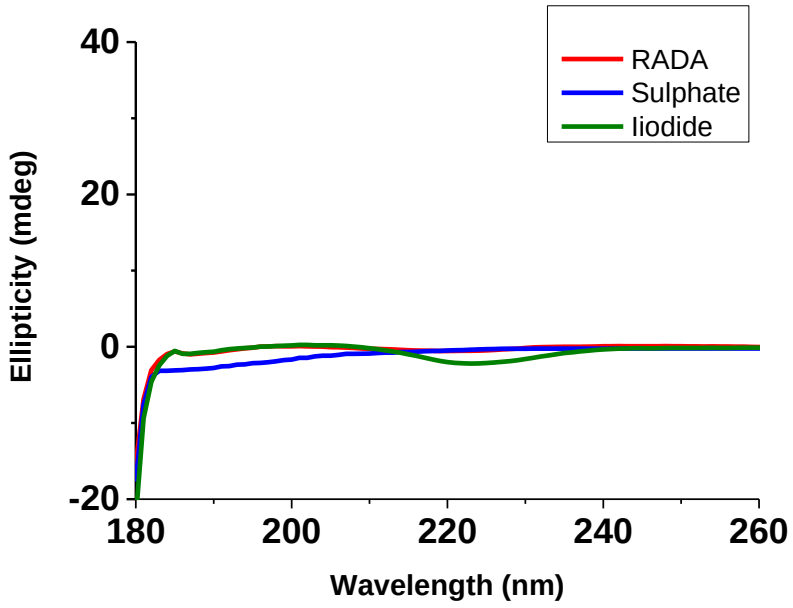

Figure 18 CD spectra of RADA16-I and RADA16-I in the presence of sodium salts of sulphate and iodide at pH 7.2 and 37˚C, day 15.

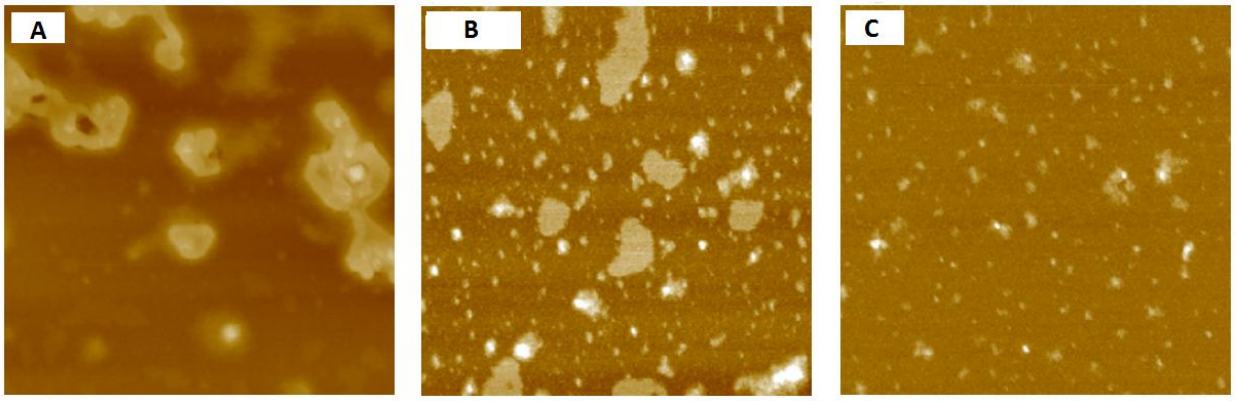

Figure 19 AFM stability study images (A), (B) and (C) washed RADA16-l, RADA16-l with sulphate, RADA16-l with iodide respectively. Scale 1µm ✕ 1µm

In order to determine whether the temperature is responsible for the instability or the change in the pH, 50 µl of RADA16-I was placed at 37 ˚C for two weeks without washing the gel. Figure 20 shows that the peptide gel is still able to form nanofibers suggesting that the instability is due to the pH change.

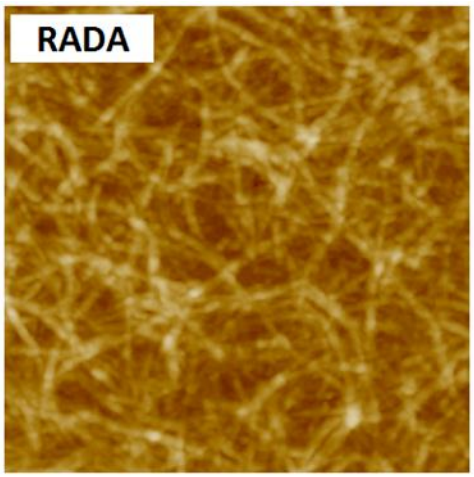

Figure 20 AFM image of RADA16-I after two weeks at 37˚C. Scale 1µm ✕ 1µm

Jun *et al.* reported that the β-sheets of oligopeptides are strongly influenced by the charge distribution along the chain [152]. Arginine has a pKa value of ~3.7 and aspartic acid's

pKa value is around 12.5. At acidic pH, the 4 aspartic acid side chains are unionised, while the 4 arginine side chains are ionised, thus, the electrostatic repulsive forces among the arginines lead to stretching in the peptide. On the other hand, RADA16-I is in its zwitterion state at alkaline pH *i.e.* the molecules have both positive and negative charges along their backbones. Consequently, the intermolecular attractive forces between the positively charged arginines and negatively charged aspartic acids become predominant causing RADA16-I to fold forming irregular structures instead of nanofibers.

3.3 Stability of the gels under the physiological conditions in the presence of paraformaldehyde (PFA)

Paraformaldehyde is used to fix cells and tissues. In this study, PFA was used as a stabiliser. Its hydroxyl group can react with the amine groups of the amino acids of RADA16-I. The CD measurements (Figure 21) illustrate that the control peptide (dash line) shows typical β-sheet structures with a minimum ellipticity at 219 nm and a maximum ellipticity at 197 nm at room temperature without washing with PBS. The chirality signals of the self-assembled peptide were still detected in the presence of PFA. However, the signal intensities were remarkably affected compared to the CD signal of the control RADA16-I.

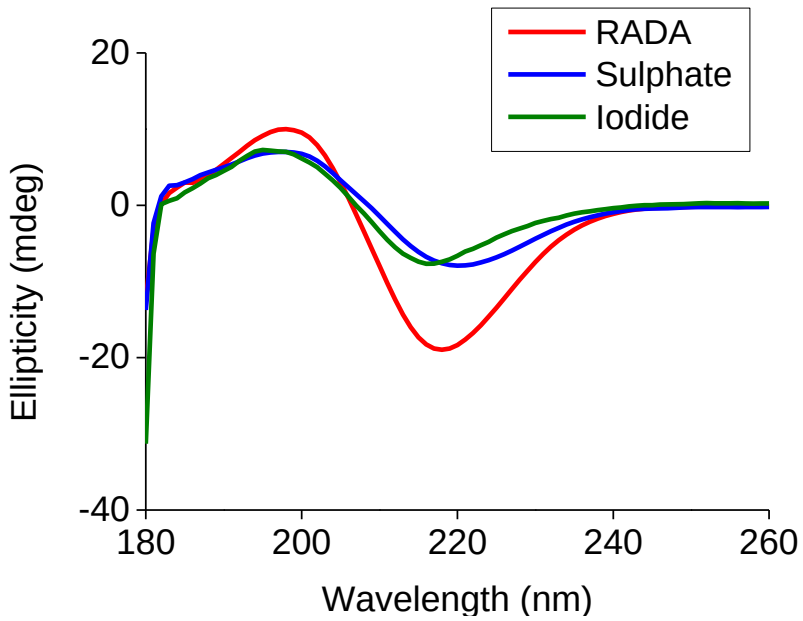

Figure 21 CD spectra of RADA16-I and RADA16-I with sodium salts of sulphate and iodide in the presence of PFA.

Typical nanostructural morphology of RADA16-I was observed (Figure 22). In the presence of sulphate, the nanofibers were highly dense and thick. Contrastingly, they are less dense and thinner in the presence of iodide. These results suggest that the formation of nanofiber structures is ion dependent.

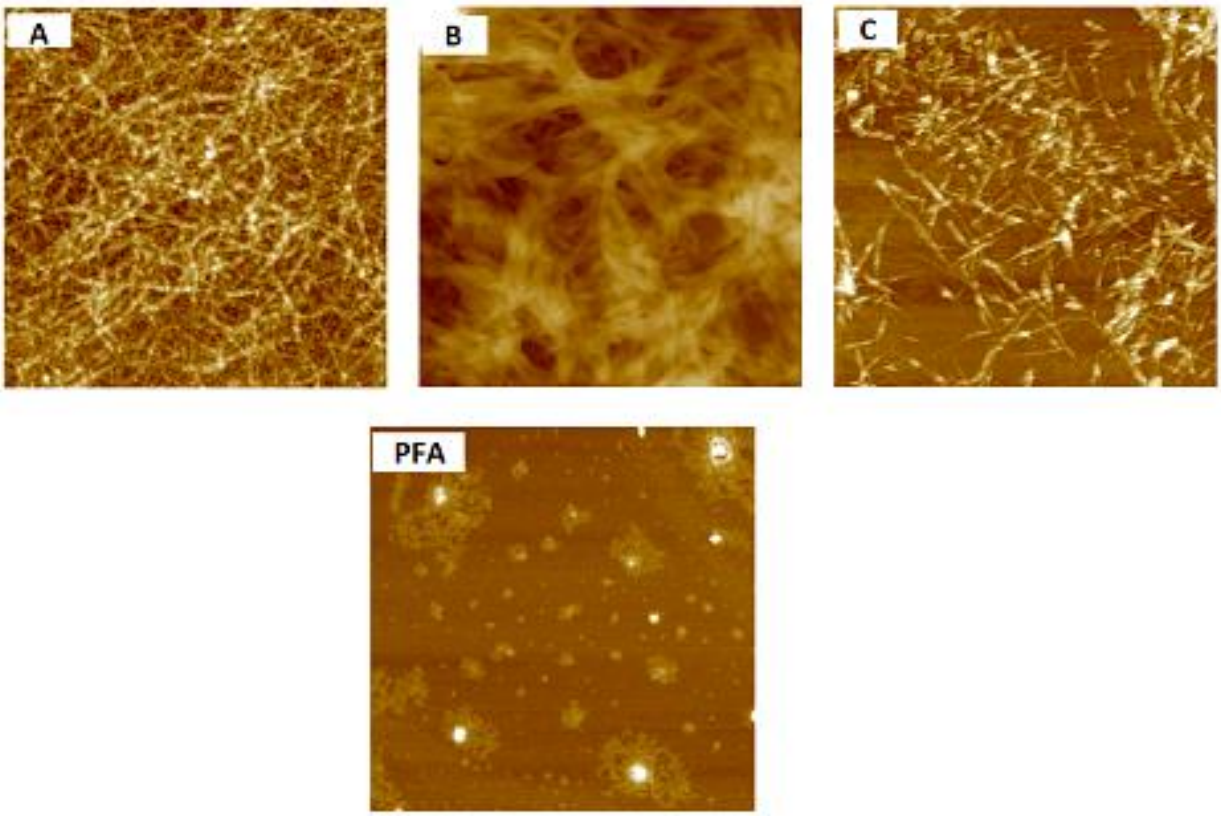

Figure 22 AFM images of RADA16-l the presence of PFA (A), with sulphate (B), with iodide (C) and PFA alone. Scale 1µm × 1µm

Again, the stability study was repeated in the presence of paraformaldehyde by placing the samples at 37˚C for 15 days with a frequent washing with PBS.

On day 15, CD was also used to investigate the gels (Figure 23). The β-sheet structures were impaired which was supported by the AFM images (Figure 24) which showed that nanofibers disappeared and different size aggregates formed instead . The stability gels formed irregular aggregates rather than nanofibers. It is obvious that the self-assembly was disrupted even in the presence of PFA.

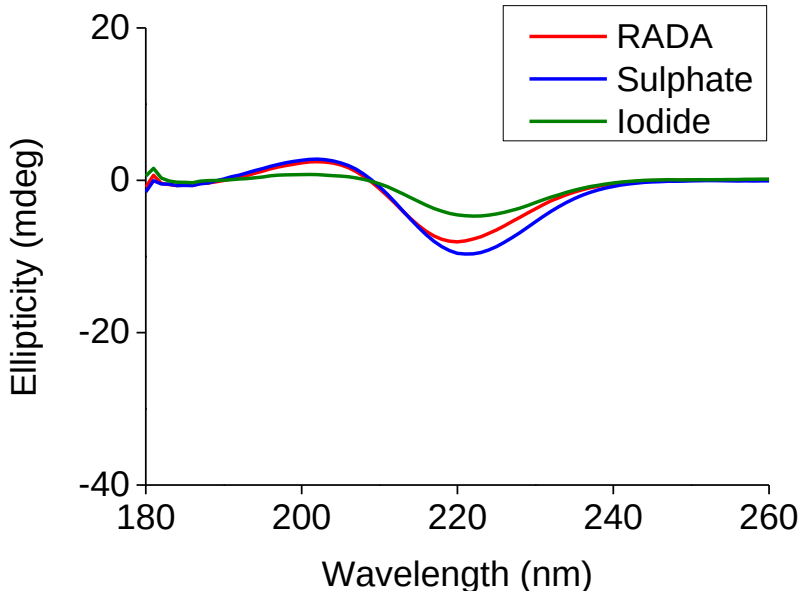

Figure 23 CD spectra of the control and stability samples on day 15 iodide in the presence of PFA.

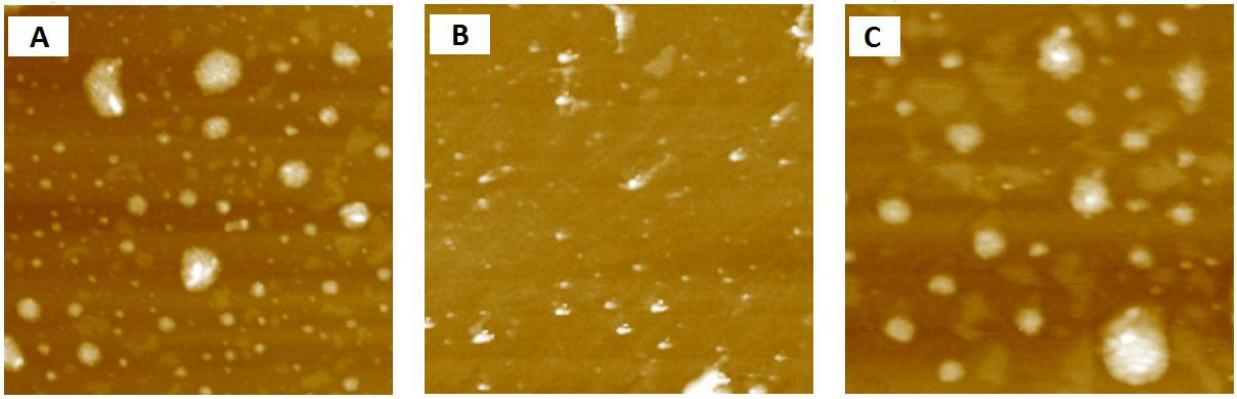

Figure 24 AFM images of the gels on day 15 of RADA16-I with PFA (A), in the presence of sulphate (B) and iodide (C). Scale 1µm ✕ 1µm

3.4 *In vitro* release of quinine from the self-assembling RADA16-I hydrogel

Quinine, an alkaloid, is used as an antimalarial drug in severe malarial infection caused by *Plasmodium falciparum* [153]. Although its mechanism of action is not fully understood, it is thought that quinine inhibits the heme detoxification pathway leading to accumulation of cytotoxic heme in the microbes leading to their death [154]. It also has analgesic, antipyretic and anti-inflammatory effects [155].

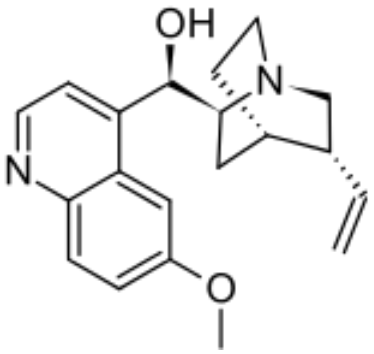

Figure 25 Chemical structure of quinine, pKa 8.7, log P 3.4, water solubility ~ 0.05 g /100 ml

Quinine is hydrophobic and is poorly soluble in water but it is soluble in organic solvents such as ethanol and acetone [157]. Self-assembling hydrogels have been widely used in drug delivery (section 1.2.3). Some researchers have used RADA16-I to slow the release of anticancer drugs and proteins, and to target specific tissue [89, 91, and 93].

The release of quinine from RADA16-I-quinine suspension was performed in PBS. The release of the drug was measured over a period of 72 hours.

The resulting release profile of quinine from RADA16, RADA16-sulphate and RADA16-iodide hydrogels are illustrated in Figure 26.

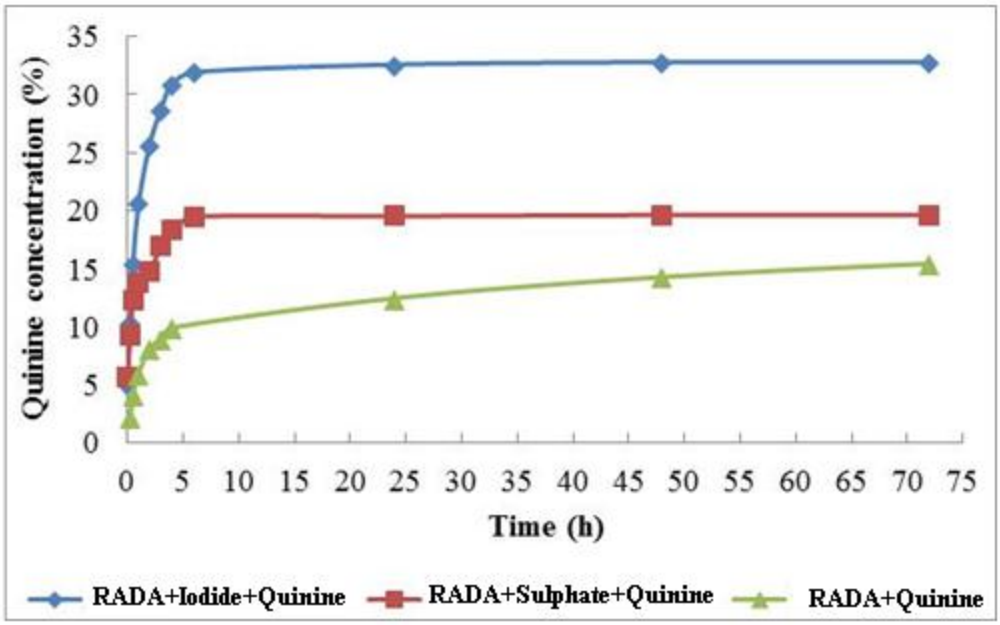

Figure 26 *In vitro* release of quinine from RADA16-I, RADA16-I-sulphate, and RADA16-I-iodide

The results of quinine release from the hydrogels showed that the RADA16-Sulphate system slowed the release of the loaded quinine. The CD results (Figure 13), FT-IR results (Figure 16) and AFM images (Figure 17) demonstrated that sulphate is a kosmotropic anion suggestion that quinine's nanoparticles were encapsulated inside the fibres and thus produced the release pattern (Figure 27). However, further study is required to prove this model and determine the location of quinine's molecules within the nanofibers. In contrast, RADA16-iodide produced faster release rates than RADA16-quinine because iodide is a gel-breaker anion (chaotropic). These results suggest that the release time of some drugs from hydrogels can be adjusted by adding specific ionic salts which can be supported by a study published by Sadeghi *et al*. who reported that ionic salts can alter the release of Ibuprofen from a pH-responsive hydrogel (Starch–Poly-Sodium-Acrylate-co-Acrylamide) [158]. Another hypothesis was proposed by Mains *et al.* in their research on the release profile of some beta-blockers from amyloid hydrogels.

They demonstrated that some drugs may act as kosmotropes or chaotropes when they add to peptide hydrogels [159].

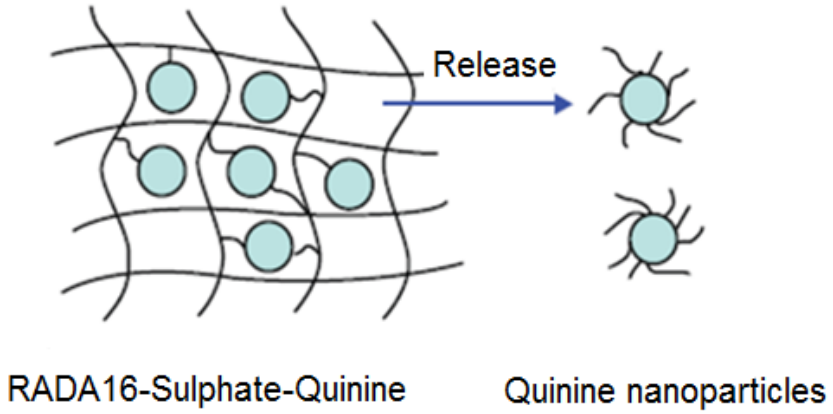

Figure 27 Schematic model for quinine release from RADA16-sulphate

3.5 The impact of the hydrogel on C3H10T1/2

Since its establishment in 1973 by Reznikoff *et al.*, cell line C3H10T1/2 (murine mesenchymal stem cells), have been widely used in stem cell research [160]. The C3H10T1/2 cells can differentiate into fibroblasts in the absence of induction. While under specific conditions, these pluripotent cells can display adipogenic [161], osteogenic [162] and chondrogenic [163] differentiation. Despite the fact that C3H10T1/2 cells have been used to study the influence of the self-assembling hydrogel scaffolds on their differentiation, their differentiation capability when they are seeded on 2-D RADA16-I hydrogel has not been investigated. In this study, the hypothesis of the effects of the salt-induced self-assembled RADA16-I hydrogel upon the osteocyte and adipocyte differentiation of the C3H10T1/2 stem cells was examined.

3.5.1 Cell density

Three different densities were examined; 1000, 5000 and 1×10^4 cells.cm^{-2} by the MTT assay. This method measures cell viability based on the ability of the mitochondrial dehydrogenase in active cells to convert the yellow MTT into blue formazan crystals [164].

It was observed (Figure 28) that 5000 cells.cm^{-2} is the best density since the growth was exponential in comparison to 10000 cells.cm^{-2} density which reached a plateau on day four and 1000 cells.cm^{-2} which showed a weak growth in the lag phase.

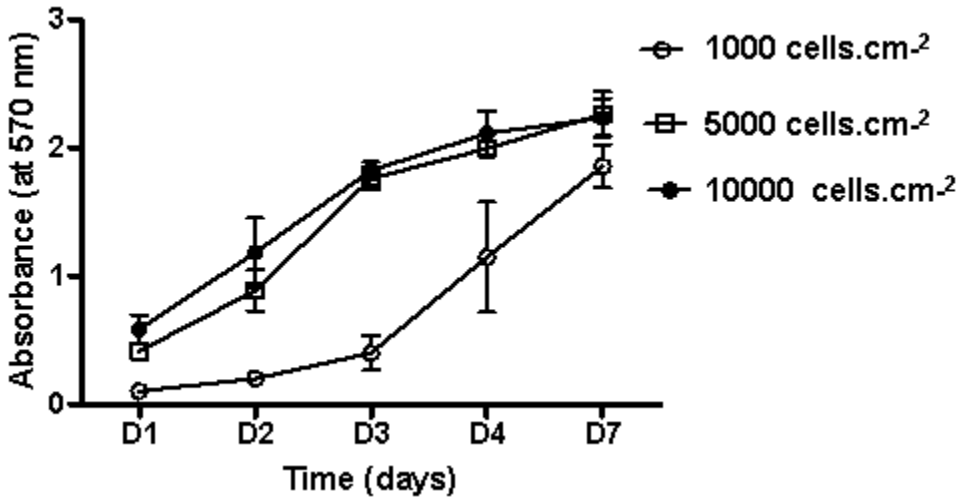

Figure 28 Growth curve of 1000, 5000 and 1×10^4 cells.cm^{-2}

3.5.2 Adipogenic differentiation

As a method to measure the adipogenic differentiation, Oil red O staining assay was performed. This stain is hydrophobic and accumulates in the fat droplets of adipocytes [165]. After two weeks in culture, the examined C3H10T1/2 cells exhibited differentiation into the adipogenic lineage when subjected to the adipocyte induction condition. The presence of the induction medium (BMP4, insulin, dexamethasone and methylisobutylxanthine) was found to increase lipid accumulation in the cells, (Figure 29-B), in contrast to the control cells without induction (Figure 29-A). Oil red O stain can be quantified. The lipid amount in adipocytes was 4.1 ± 0.4 (mean ± standard deviation SD) fold greater than that in the control cells (Figure 30)

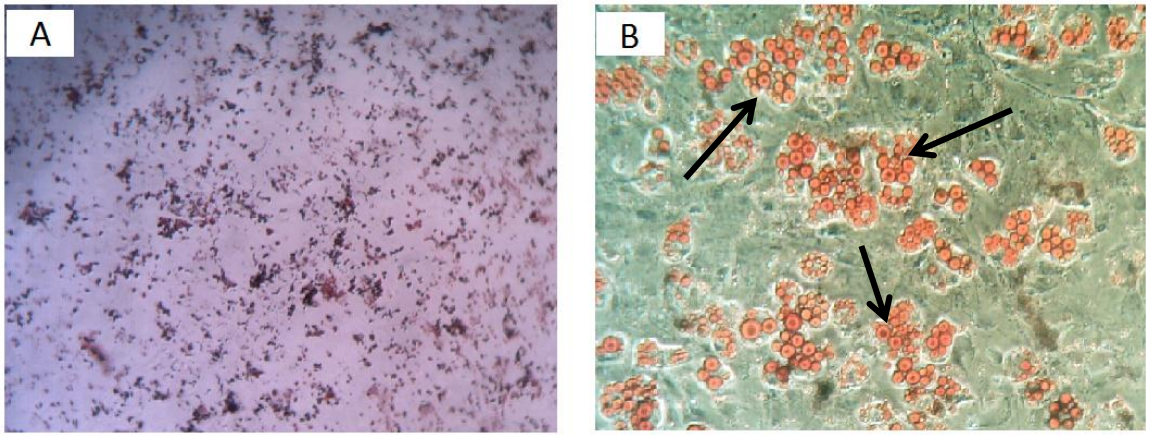

Figure 29 Light micrographs (at 20✕ objective lens magnification) of the stained cells with Oil Red O stain, without induction medium (A) and with induction medium. Arrowheads indicate lipid droplets in adipocytes.

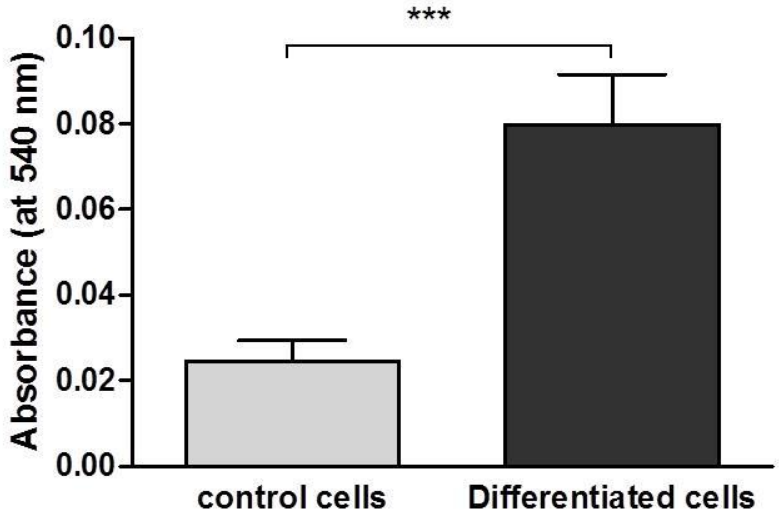

Figure 30 Oil red O staining of C3H10T1/2. The retained dye was measured at 540 nm and is shown on the y-axis (mean ± SD). The significance of the variation in the results was analysed by unpaired T-test with a significant difference at ***p<0.001.

These results agree with the findings of Tang *et al.* [161] and Huang *et al.* [166] who found that bone morphogenic protein 4 (BMP4) triggers the commitment of C3H10T1/2 cells to the adipocyte lineage. Also, in agreement with this study, Lee *et al.* [167] and Lim *et al.* [168] reported that insulin, dexamethasone and methylisobutylxanthine cocktail can be used with BMP4 to increase the capability of the cells to differentiate to adipocytes.

3.5.3 Osteogenic differentiation

The C3H10T1/2 cells showed osteogenic differentiation under the co-treatment with retinoic acid, ascorbic acid, β-glycerophosphate and dexamethasone for 28 days. The minerlisation matrices of the cells were positive for Von Kossa staining. In this method, the reduced calcium is replaced with silver deposits (silver nitrate) which can be

visualised as metallic silver. Here, the deposits (Figure 31-B) were stained black indicating the osteogenic differentiation compared with the control cells showed in (Figure 31-A).

Alkaline phosphatase (ALP) enzyme activity is a good indicator of the osteogenic differentiation of mesenchymal stem cells. Control cells, without induction, exhibited weak ALP activity in comparison to that of induced cells where a significant increase (~ 13-fold) was observed, Figure 32.

In previous studies performed by Zhao *et al.* [169], Cho *et al.* [170] and Bone *et al.* [171], C3H10T1/2 cells treated with the osteogenic induction cocktail (ascorbic acid, β-glycerophosphate and dexamethasone) exhibited osteogenic differentiation which agree with findings of this experiment.

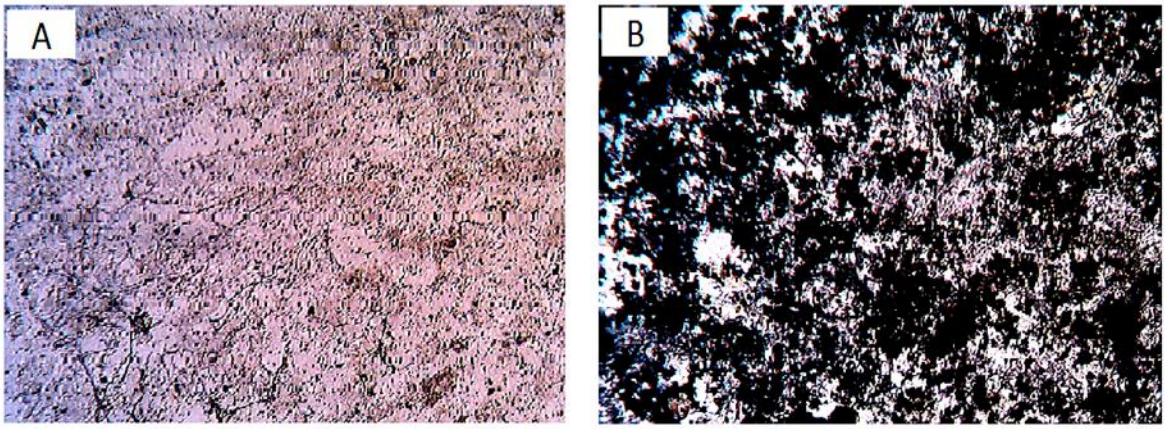

Figure 31 Light micrographs of the osteogenic induced C3H10T1/2 cells (A) and control cells without induction (B), taken with 20✕ objective lens magnification, stained with Von Kossa stain

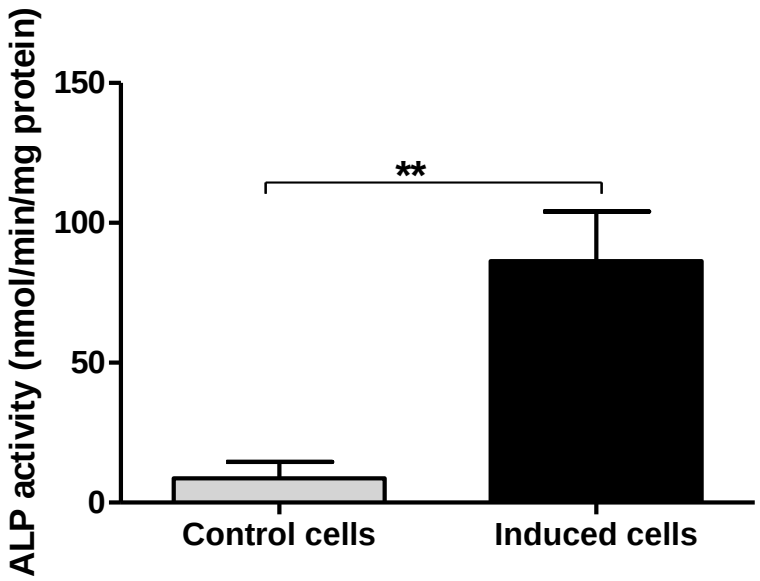

Figure 32 Alkaline phosphatase (ALP) activity of the control and induced cells. It was quantified using *p*-nitrophenol phosphate as substrate, and the measurements were normalised to the total protein. The significance of the variation in the results was analysed by unpaired T-test with a significant difference at **p<0.01.

3.5.4 Evaluation of C3H10T1/2 proliferation on the hydrogels

C3H10T1/2 cells were seeded on the hydrogels; RADA16-I (R), RADA16-I and sodium sulphate (R-S), RADA16-I and sodium iodide (R-I), RADA16-I and paraformaldehyde (R-PFA), R-PFA and sodium sulphate (R-PFA-S), R-PFA and sodium iodide (R-PFA-I), and wells washed with paraformaldehyde (PFA). Control refers to cells seeded on plasma treated polystyrene 96-well plate without any additions. The same initial density, 5000 cell/cm^2, was plated and the cells were left to proliferate for 24 hours then Alamar blue measurements (Figure 33) were obtained on day 1, 2, 3, 6 and 7. This assay measures the cell viability where metabolically active cells convert resazurin to a fluorescent compound that can be quantified spectroscopically [172]. It can be seen that the cells did not expand, in comparison to the cells in the absence of RADA16-I, PFA and/or salts,

which showed an exponential growth. The results suggested that PFA is cytotoxic, and RADA16-I and/or the salts are also cytotoxic, therefore, further experiments were carried out to determine whether the toxicity is due to the hydrogel, salts, or both.

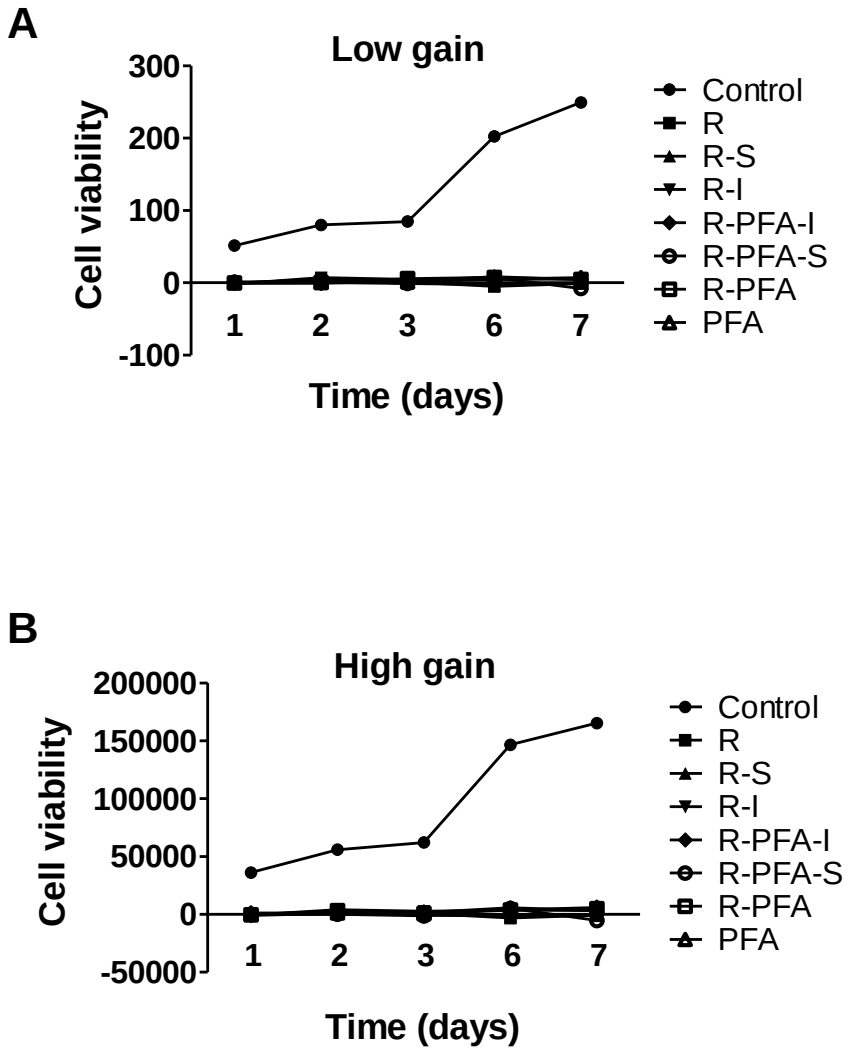

Figure 33 Proliferation of C3H10T1/2 on the hydrogels quantified by Alamar blue assay low gain (A) and high gain (B) on day 1,2,3,6 and 7.

3.5.5 C3H10T1/2 cell adhesion

To examine if the cells did not proliferate due to their attachment failure, fibronectin (FN) was used to enhance the cell attachment on the hydrogel (Figure 34). Fibronectin is an adhesive glycoprotein of the ECM involved in many cellular processes including attachment, migration, blood clotting and metastasis [173]. In cell adhesion, its subunits bind to specific structures in the extracellular matrix and on cell surfaces such as fibrin, heparin and collagen. The arginine-glycine-aspartate sequence (RGD) is responsible for the binding activity with receptors found on the surfaces of the cells and it is also recognised by different surface integrins [174].

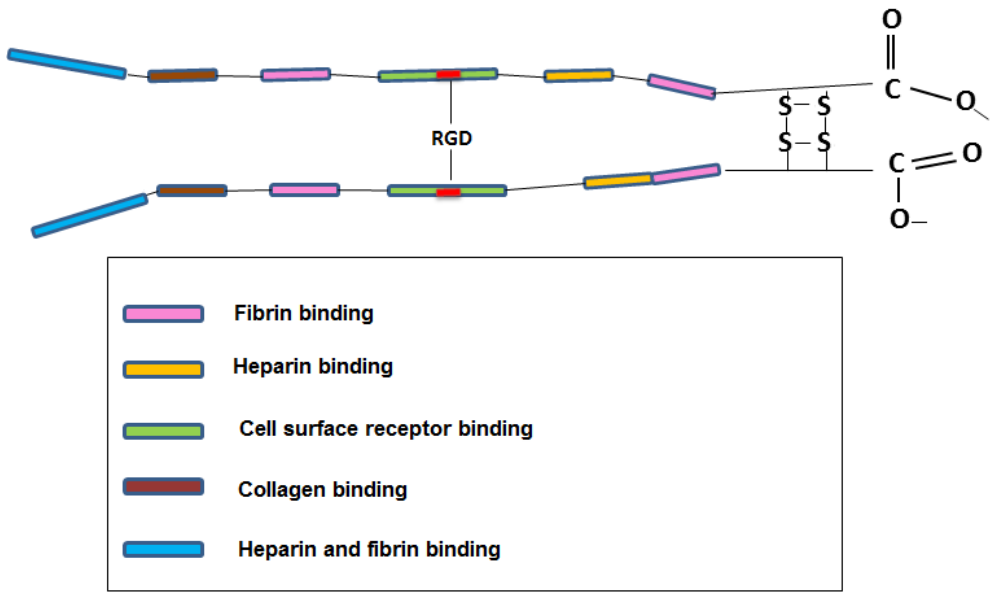

Figure 34 Fibronectin's structure, adapted from, adapted from [175]

Figure 35 shows the cell viability in presence of different concentrations of FN. The results indicated that material exhibited low toxicity, and the cells were able to expand and grow on the hydrogel. Increasing the FN concentration led to better viability. These

results revealed that the RADA16-I did not significantly damage the cells, and the decrease in the cells could be related to the salts used.

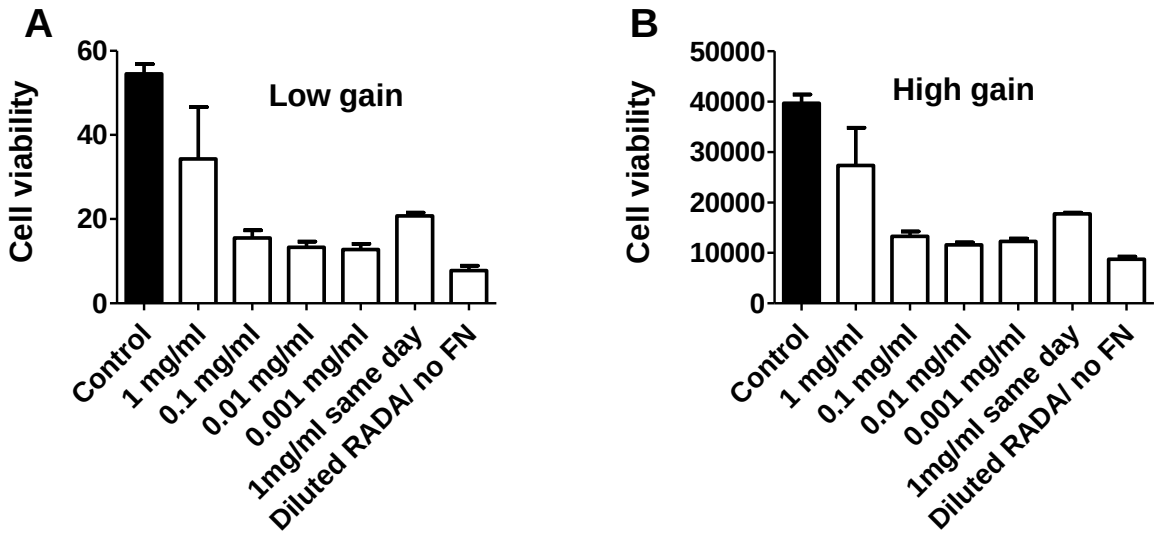

Figure 35 Cell viability in the presence of different FN concentrations added on the gels 48 after seeding

3.5.6 *In vitro* salt toxicity study

The fibronectin-induced binding experiment proved that RADA16-I is biocompatible. To evaluate the effects of the cells exposure to the salts (sodium sulphate and sodium iodide), different concentrations were prepared, sterilised and added to wells containing the C3H10T1/2 cells grown for 24 hours at a density of 5000 cell.cm-^{2}. The cell viability was measured by MTT essay after 72 hours. Figure 36 illustrates the viability of the cells in the presence of the salts. A concentration-dependant decrease trend in the stem cell counts is observed for both salts. This reduction is most pronounced at higher concentrations.

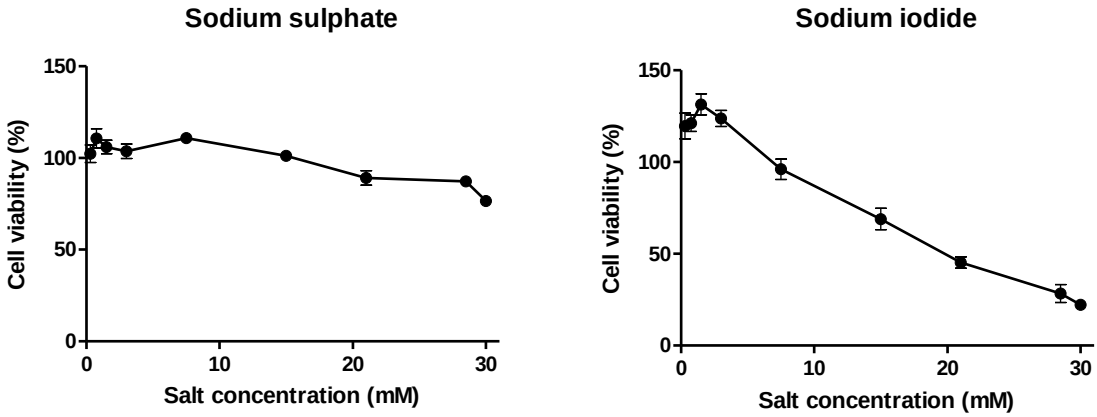

Figure 36 viability of C3H10T1/2 obtained by the MTT assay (at 570 nm) after incubation for 72 hour with different concentrations of sodium sulphate and sodium iodide salts (mM)

In order to investigate whether mixing of the salts with the hydrogels can minimise the cytotoxicity of the salts or not, samples were prepared as described in 4.4 with two modifications. PFA was washed with a 0.3 M glycine (in PBS) solution to quench the PFA. Secondly, a 0.01mg.ml^{-1} FN solution (50 µl per well) was added. The proliferation of the cells was measured using Alamar blue proliferation assay. The comparison between the viability of the cells seeded on the hydrogels and the control cells plated on plasma treated polystyrene indicates that the salts killed the cells at the used concentration (600 mM) even when they were mixed with the hydrogel (Figure 37). The PFA was also toxic and glycine did not diminish its cytotoxicity.

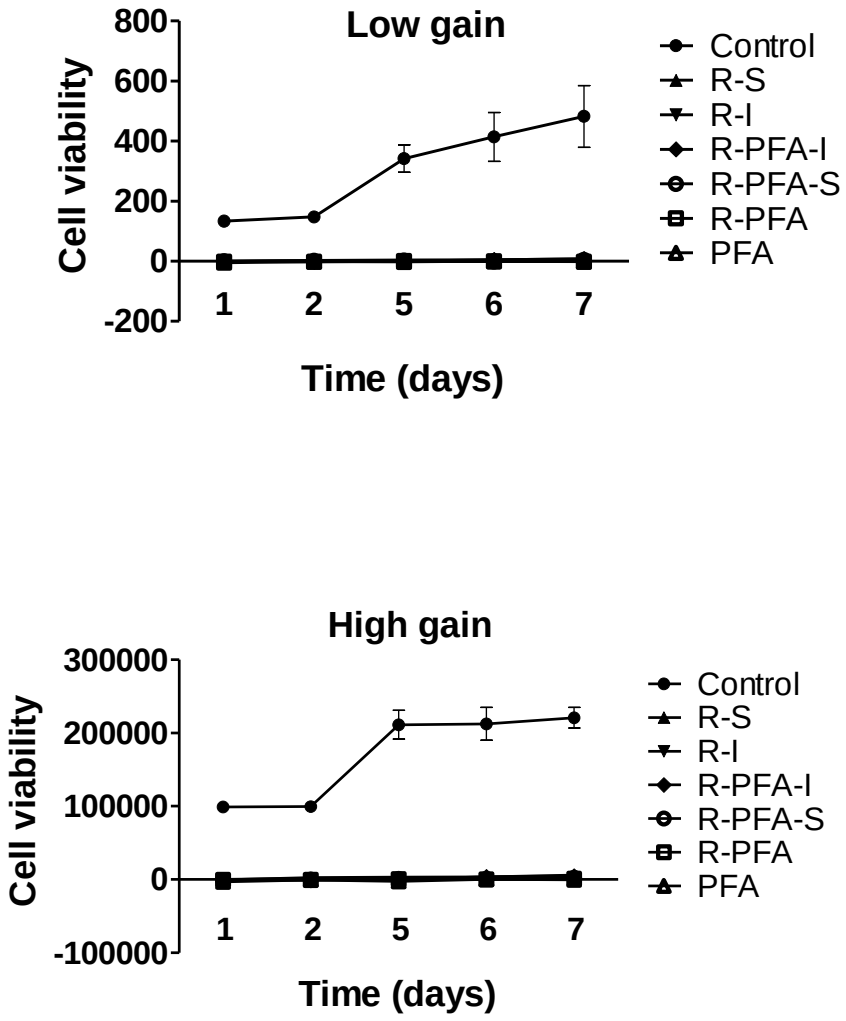

Figure 37 Proliferation of C3H10T1/2 on the hydrogels in the presence of the salts and 0.01mg/ml FN, quantified by Alamar blue assay, low gain and high gain on day,1,2,5,6 and 7(n=6).

Finally, different sulphate and iodide sodium salts (e.g. 10, 100, 300 and 600 mM) solutions were used to evaluate the cytotoxicity at low concentrations. Again, the cells failed to expand even with lower salt concentrations, Figure 38.

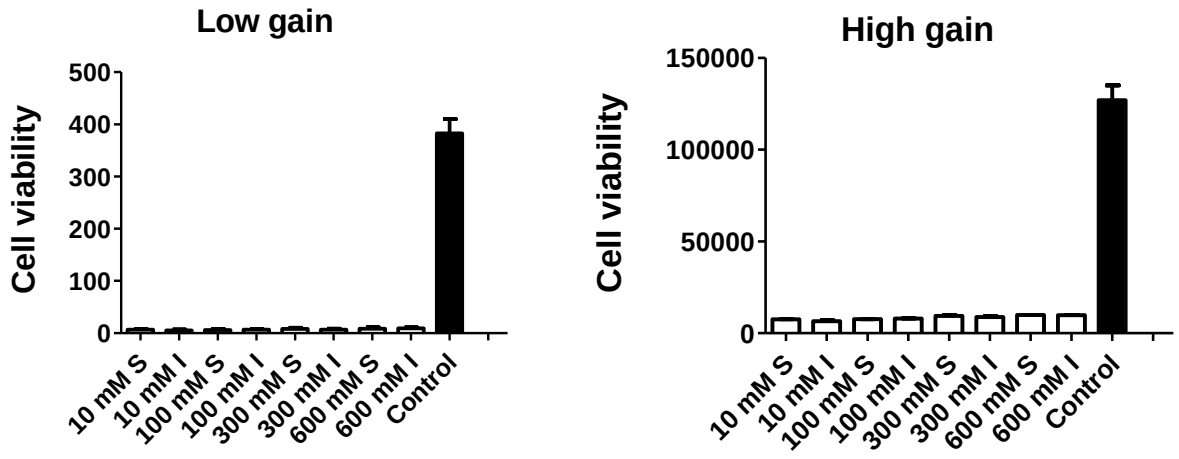

Figure 38 cell viability in the presence of 0.01 mg/ml FN and different salt concentrations, day 7.

The results of the cytotoxicity experiments clearly showed that PFA, sulphate and iodide ions have intrinsic adverse effects on C3H10T1/2 cells even at their minimum concentrations. Previous reports have shown that C3H10T1/2 cells can be cultured in self-assembling peptide scaffolds. Seo *et al*. demonstrated that the osteogenic differentiation of this cell line can be induced by culturing on the tailor-made micropit surfaces that enhanced focal adhesion and intracellular actin polymerisation of the cells [176]. In another study, Inagaki *et al*. reported that C3H10T1/2 cells cultured on a synthetic double-network hydrogel, which is composed of poly-(2-acrylamido-2-methylpropanesulphonic acid), created focal adhesions, aggregated and developed into large nodules within one week and expressed more type II collagen at the protein level when compared with cells cultured on polystyrene dishes [177].

With regards to RADA16-I without the ionic salts, no significant cytotoxic effect for the hydrogel on the cells was observed (Figure 35). Previous investigators have reported that

RADA16-I can support attachment, proliferation and differentiation of both stromal and stem cells. For example, Hamada *et al.* showed that RADA16-I supports the attachment of MSCs isolated from rat bone marrow and encapsulated in the peptide, and induces the osteogenic differentiation *in vitro* in the presence of induction medium (β-glycophospahte, ascorbic acid and dexamethasone) [110]. Erickson *et al.* demonstrated that RADA16-I can promote bovine MSCs to undergo chondrogenesis when the cells are encapsulated in the hydrogel [111]. In their work, Matsumoto *et al.* reported that hydroxyapatite ceramics can be incorporated into MSCs/ RADA16-I to form MSCs/ RADA16-I/ hydroxyapatite ceramics composites. These composites enhanced the mechanical properties of the ECM and directed the MSCs toward osteogenesis differentiation [112].

Based on the results of this study which demonstrate that C3H10T1/2 cells cultured on RADA16-I failed to prolifirate in the presence of the sodium salts of iodide and sulphate, it can be concluded that triggering the self-assembly of hydrogels with ionic salts might not be a good approach for biomedical applications due to the instability of the nanostructures formed and cytotoxicity. The formation of RADA16-I hydrogel with other macromolecules, such as sugars and amino acid motifs, is an alternative method to eliminate the disadvantages of residual chemicals.

Conclusions

Stimuli-responsive self-assembling peptide hydrogels are promising materials with a broad range of potential applications in biomedical research fields such as drug delivery systems and tissue engineering. This research focused on the impact of anionic salts (Hofmeister series) on the self-assembly of RADA16-I. This peptide was shown to self-assemble and form nanoscale fibres. The AFM, CD and FT-IR results showed that anions remarkably influence the nanostructure of RADA16-I. The β-sheet fibres were unstable at the neutral pH. Quinine was chosen a model for hydrophobic drugs. The quinine release experiment demonstrated that such approach can provide means for controlled drug release. Murine C3H10T1/2 stem cells were used to assess the biocompatibility of the hydrogels under 2-D scaffold conditions, particularly looking into the adipogenic and osteogenic linage differentiation of the cells. The cell culture resulted in poor viability due the cytotoxicity of sodium sulphate and sodium iodide.

In conclusion, ionic salts, such as sodium sulphate and sodium iodide, have a dramatic influence on RADA16-I hydrogel. The self-assembling β-sheet nanofibers were significantly affected leading to different nanomorphologies. This cost-effective method can be used to tailor different mechanical properties of peptide hydrogels in order to control the release of drugs and other bioactive molecules. However, the instability of the nanostructures at the physiological pH has to be addressed. Finally, the cytotoxic effect of the salts on the C3H10T1/2 stem cells suggested that conjugation of RADA16-I with other macromolecules, such as polymers and amino acid motifs, is an alternative method to eliminate the disadvantages of residual chemicals.

References

1. Nelson, D. L., & Cox, M. M. (2004). *Lehninger principles of biochemistry (4th ed.).* New York, USA: W. H. Freeman.

2. Hoare, T. R., & Kohane, D. S. (2008). Hydrogels in drug delivery: progress and challenges. *Polymer*. *49*, 1993-2007.

3. Lee, K. Y., & Mooney, D. J. (2001). Hydrogels for tissue engineering. *Chemical Reviews*, *101*(7), 1869–1880.

4. Chen, P. (2005). Self-assembly of ionic-complementary peptides: a physicochemical viewpoint. *Colloids and Surfaces A: Physicochemical and Engineering Aspects*, *261*(1-3), 3–24.

5. Cormier, A. R., Ruiz-Orta, C., Alamo, R. G., & Paravastu, A. K. (2012). Solid state self-assembly mechanism of RADA16-I designer peptide. *Biomacromolecules*, *13*(6), 1794–804.

6. Yokoi, H., Kinoshita, T., & Zhang, S. (2005). Dynamic reassembly of peptide RADA16 nanofiber scaffold. *Proceedings of the National Academy of Sciences of the United States of America*, *102*(24), 8414–9.

7. Sun, L., & Zhao, X. (2012). A self-assembling peptide RADA16-I integrated with spider fibroin uncrystalline motifs. *International Journal of Nanomedicine*, *7*, 571–80.

8. Zhang, H., Luo, H., & Zhao, X. (2010). Mechanistic study of self-assembling peptide RADA16-I in formation of nanofibers and hydrogels. *Journal of Nanotechnology in Engineering and Medicine*, *1*(1), 011007.

9. Ellis-behnke, R., & Zhao, X. (2008). Temperature and pH effects on biophysical and morphological properties of self-assembling peptide, *Journal of peptide science*, (*January*), 152–162.

10. Cheng, T.-Y., Wu, H.-C., Huang, M.-Y., Chang, W.-H., Lee, C.-H., & Wang, T.-W. (2013). Self-assembling functionalized nanopeptides for immediate hemostasis and accelerative liver tissue regeneration. *Nanoscale*, *5*(7), 2734–44.

11. Arosio, P., Owczarz, M., Wu, H., Butté, A., & Morbidelli, M. (2012a). End-to-end self-assembly of RADA 16-I nanofibrils in aqueous solutions. *Biophysical Journal*, *102*, 1617–1626.

12. Lim, D., & Wichterle, O. (1960). Hydrophilic gels for biological use. *Nature*. *185*, 117-118.

13. Weiss, P., Fatimi, A., Guicheux, J., & Vinatier, C. (2010). Biomedical applications of hydrogels. *Business*, *C*, 247–268.

14. Jun Loh, X., & A. Scherman, O. (2013). *Polymeric and self assembled hydrogels: from fundamental understanding to applications*. Dorchester, UK: Henry Ling Limited.

15. Peppas, N. a., Hilt, J. Z., Khademhosseini, A., Langer, R., & Peppas, B. N. A. (2006). Hydrogels in biology and medicine: from molecular principles to bionanotechnology. *Advanced Materials*, *18*, 1345–1360.

16. Huang, Y., Qiu, Z., Xu, Y., Shi, J., Lin, H., & Zhang, Y. (2011). Supramolecular hydrogels based on short peptides linked with conformational switch. *Organic & Biomolecular Chemistry*, *9*, 2149–2155.

17. Suzuki, Y., Tanihara, M., Nishimura, Y., Suzuki, K., Kakimaru, Y., & Shimizu, Y. (1998). A new drug delivery system with controlled release of antibiotic only in the presence of infection. *Journal of Biomedical Materials Research*, *42*, 112–116.

18. Tasaki, I. (2005). Repetitive abrupt structural changes in polyanionic gels: a comparison with analogous processes in nerve fibers. *Journal of Theoretical Biology*, *236*, 2–11.

19. Gelain, F., Horii, A., & Zhang, S. (2007). Designer self-assembling peptide scaffolds for 3-d tissue cell cultures and regenerative medicine. *Macromolecular Bioscience*, *7*(5), 544–51.

20. Borzacchiello, A., & Ambrosio, L. (2009). Structure-property relationships in hydrogels. *Biophysical Journal*, *28*, *9-20.*

21. De la Torre, P. M., Torrado, S., & Torrado, S. (2003). Interpolymer complexes of poly(acrylic acid) and chitosan: influence of the ionic hydrogel-forming medium. *Biomaterials*, *24*, 1459–1468.

22. Bajpai, S. K. (2001). Swelling-deswelling behavior of poly(acrylamide-co-maleic acid) hydrogels. *Journal of Applied Polymer Science*, *80*, 2782–2789.

23. Peppas, N. A., Huang, Y., Torres-Lugo, M., Ward, J. H., & Zhang, J. (2000). Physicochemical foundations and structural design of hydrogels in medicine and biology. *Annual Review of Biomedical Engineering*, 2, 9–29.

24. Miller, D. R., & Peppas, N. A. (1986). Bulk characterization and scanning electron microscopy of hydrogels of P(VA-co-NVP). *Biomaterials*, *7*, 329–339.

25. Gulrez, S. K., Al-Assaf, S., & Phillips, G. O. (2011). Hydrogels: methods of preparation, characterisation and applications. *Progress in Molecular and Environmental Bioengineering*, *5*, 117–150.

26. Hoffman, A. S. (2012). Hydrogels for biomedical applications. *Advanced Drug Delivery Reviews*. 15, 208-220.

27. Gupta, P., Vermani, K., & Garg, S. (2002). Hydrogels: from controlled release to pH-responsive drug delivery. *Drug Discovery Today*, *7*, 569–579.

28. Kamath, K. R., & Park, K. (1993). Biodegradable hydrogels in drug delivery. *Advanced Drug Delivery Reviews*. *64*, 49-60.

29. Peppas, N. A., Bures, P., Leobandung, W., & Ichikawa, H. (2000). Hydrogels in pharmaceutical formulations. *European Journal of Pharmaceutics and Biopharmaceutics*, *50*, 27–46.

30. Halperin, A., Tirrell, M., & Lodge, T. P. (1992). Tethered chains in polymer microstructures. *Advances in Polymer Science*, *100*, 31–71.

31. Luo, Z., Wang, S., & Zhang, S. (2011). Fabrication of self-assembling d-form peptide nanofiber scaffold d-EAK16 for rapid hemostasis. *Biomaterials*, *32*, 2013–2020.

32. Xinming, L., Yingde, C., Lloyd, A. W., Mikhalovsky, S. V., Sandeman, S. R., Howel, C. A., & Liewen, L. (2008). Polymeric hydrogels for novel contact lens-based ophthalmic drug delivery systems: A review. *Contact Lens and Anterior Eye*. *31(*2), 57-64.

33. Chen, L., Revel, S., Morris, K., & Adams, D. J. (2010). Energy transfer in self-assembled dipeptide hydrogels. *Chemical Communications (Cambridge, England)*, *46*(24), 4267–9.

34. Chan, K. W. Y., Liu, G., Song, X., Kim, H., Yu, T., Arifin, D. R., & McMahon, M. T. (2013). MRI-detectable pH nanosensors incorporated into hydrogels for in vivo sensing of transplanted-cell viability. *Nature Materials*, *12*, 268–75.

35. Fisher, M. B., & Mauck, R. L. (2013). Tissue engineering and regenerative medicine: recent innovations and the transition to translation. *Tissue Engineering. Part B, Reviews*, *19*, 1–13.

36. Chua, C. K., Tan, L. P., & An, J. (2013). Advanced nanobiomaterials for tissue engineering and regenerative medicine. *Nanomedicine*, *8*(4), 501–3.

37. Macchiarini, P., Jungebluth, P., Go, T., Asnaghi, M. A., Rees, L. E., Cogan, T. A., & Birchall, M. A. (2008). Clinical transplantation of a tissue-engineered airway. *The Lancet*, *372*, 2023–2030.

38. Song, J. J., Guyette, J. P., Gilpin, S. E., Gonzalez, G., Vacanti, J. P., & Ott, H. C. (2013). Regeneration and experimental orthotopic transplantation of a bioengineered kidney. *Nature Medicine*, *19*, 646–51.

39. Lee, S. J., & Atala, A. (2013). Scaffold technologies for controlling cell behavior in tissue engineering. *Biomedical Materials*, *8*, 010201.

40. Amosi, N., Zarzhitsky, S., Gilsohn, E., Salnikov, O., Monsonego-Ornan, E., Shahar, R., & Rapaport, H. (2012). Acidic peptide hydrogel scaffolds enhance calcium phosphate mineral turnover into bone tissue. *Acta Biomaterialia*, *8*, 2466–2475.

41. Gayet, J.-C., & Fortier, G. (1996). High water content BSA-PEG hydrogel for controlled release device: evaluation of the drug release properties. *Journal of Controlled Release*, *38*(2), 177–184.

42. Schild, H. G. (1992). Poly(N-isopropylacrylamide): experiment , theory and application. *Progress in Polymer Science*, *17*, 163–249.

43. Suwa, K., Morishita, A., Akashi, M. (1997). Synthesis and functionalities of poly(N-vinylalkylamide). V. control of a lower critical solution temperature of poly(N-vinylalkylamide). *J. Polym. Sci. Part A Polym. Chem.*, *35*, 3087–3094.

44. He, C., Kim, S. W., & Lee, D. S. (2008). In situ gelling stimuli-sensitive block copolymer hydrogels for drug delivery. *Journal of Controlled Release*, *127*, 189-207.

45. Wu, J., Wei, W., Wang, L. Y., Su, Z. G., & Ma, G. H. (2007). A thermosensitive hydrogel based on quaternized chitosan and poly(ethylene glycol) for nasal drug delivery system. *Biomaterials*, *28*, 2220–2232.

46. Mahkam, M. (2010). Novel pH-sensitive hydrogels for colon-specific drug delivery. *Drug Delivery*, *17*, 158–163.

47. Eddington, D. T., & Beebe, D. J. (2004). Flow control with hydrogels. *Advanced Drug Delivery Reviews*, *56*, 199-210.

48. Dayananda, K., He, C., & Lee, D. S. (2008). In situ gelling aqueous solutions of pH- and temperature-sensitive poly(ester amino urethane)s. *Polymer*, *49*, 4620–4625.

49. Smith, J. R., & Lamprou, D. a. (2014). Polymer coatings for biomedical applications: a review. *Transactions of the IMF*, *92*(1), 9–19.

50. Alberts, B., Johnson, A., Lewis, J., Raff, M., Roberts, K., & Walter, P. (2002). *Molecular Biology of the Cell (4th Edition).* New York, USA: Garland Science.

51. Smith, D. K. (2009). Lost in translation? Chirality effects in the self-assembly of nanostructured gel-phase materials. *Chemical Society Reviews*, *38*(3), 684–94.

52. Brizard, A., Oda, R., & Huc, I. (2005). Chirality effects in self-assembled Fibrillar networks. *Topics in Current Chemistry*, *256*, 167–218.

53. Kol, N., Adler-Abramovich, L., Barlam, D., Shneck, R. Z., Gazit, E., & Rousso, I. (2005). Self-assembled peptide nanotubes are uniquely rigid bioinspired supramolecular structures. *Nano Letters*, *5*, 1343–1346.

54. Reches, M., & Gazit, E. (2006). Controlled patterning of aligned self-assembled peptide nanotubes. *Nature Nanotechnology*, *1*, 195-200.

55. Isidro-Llobet, A., Alvarez, M., & Albericio, F. (2009). Amino acid-protecting groups. *Chemical Reviews*, *109*(6), 2455–504.

56. Johnson, E. K., Adams, D. J., & Cameron, P. J. (2011). Peptide based low molecular weight gelators. *Journal of Materials Chemistry*, *21*(7), 2024.

57. Fung, S. Y., Keyes, C., Duhamel, J., & Chen, P. (2003). Concentration effect on the aggregation of a self-assembling oligopeptide. *Biophysical Journal*, *85*, 537–548.

58. Saiani, A., Mohammed, A., Frielinghaus, H., Collins, R., Hodson, N., Kielty, C.M., Sherratt, M.J., & Miller, A.F. (2009). Self-assembly and gelation properties of [small alpha]-helix versus [small beta]-sheet forming peptides. *Soft MatteR*, *5*(1), 193-202.

59. Bowerman, C. J., Ryan, D. M., Nissan, D. A., & Nilsson, B. L. (2009). The effect of increasing hydrophobicity on the self-assembly of amphipathic beta-sheet peptides. *Molecular bioSystems*, *5*, 1058–1069.

60. Aggeli, A., Nyrkova, I. A., Bell, M., Harding, R., Carrick, L., McLeish, T. C., & Boden, N. (2001). Hierarchical self-assembly of chiral rod-like molecules as a model for peptide beta -sheet tapes, ribbons, fibrils, and fibers. *Proceedings of the National Academy of Sciences of the United States of America*, *98*, 11857–11862.

61. Whitesides, G. M., Mathias, J. P., & Seto, C. T. (1991). Molecular self-assembly and nanochemistry: a chemical strategy for the synthesis of nanostructures. *Science*, *254*(5036), 1312–9.

62. Hartgerink, J. D., Beniash, E., & Stupp, S. I. (2002). Peptide-amphiphile nanofibers: a versatile scaffold for the preparation of self-assembling materials. *Proceedings of the National Academy of Sciences of the United States of America*, *99*, 5133–5138.

63. Hartgerink, J. D., Beniash, E., & Stupp, S. I. (2001). Self-assembly and mineralization of peptide-amphiphile nanofibers. *Science*, *294*, 1684–1688.

64. Boyle, A. L., & Woolfson, D. N. (2011). De novo designed peptides for biological applications. *Chemical Society Reviews*, *40*, 4295–4306.

65. Woolfson, D. N. (2010). Building fibrous biomaterials from alpha-helical and collagen-like coiled-coil peptides. *Biopolymers*, *94*, 118–127.

66. Tang, C., Smith, A. M., Collins, R. F., Ulijn, R. V, & Saiani, A. (2009). Fmoc-diphenylalanine self-assembly mechanism induces apparent pKa shifts. *Langmuir : The ACS Journal of Surfaces and Colloids*, *25*, 9447–9453.

67. Smith, a. M., Williams, R. J., Tang, C., Coppo, P., Collins, R. F., Turner, M. L., & Ulijn, R. V. (2008). Fmoc-diphenylalanine self assembles to a hydrogel via a novel architecture based on π–π interlocked β-sheets. *Advanced Materials*, *20*(1), 37–41.

68. Rajagopal, K., Ozbas, B., Pochan, D. J., & Schneider, J. P. (2006). Probing the importance of lateral hydrophobic association in self-assembling peptide hydrogelators. *European Biophysics Journal*, *35*, 162–169.

69. Branco, M. C., Nettesheim, F., Pochan, D. J., Schneider, J. P., & Wagner, N. J. (2009). Fast dynamics of semiflexible chain networks of self-assembled peptides. *Biomacromolecules*, *10*, 1374–1380.

70. Zhang, S., Holmes, T., Lockshin, C., & Rich, A. (1993). Spontaneous assembly of a self-complementary oligopeptide to form a stable macroscopic membrane. *Proceedings of the National Academy of Sciences of the United States of America*, *90*, 3334–3338.

71. Zhang, S. (2003). Building from the bottom up. *Materials Today*, *6*, 20-27.

72. Zhang, S. (2002). Emerging biological materials through molecular self-assembly. *Biotechnology Advances*, *20*, 321–339.

73. Zhanga, S., Lin, Y., Altman, M., Lässle, M., Nugent, H., Frankel, F., & Rich, A. (1999). Biological surface engineering: A simple system for cell pattern formation. *Biomaterials*, *20*, 1213–1220.

74. Zhang, S. (2002). Emerging biological materials through molecular self-assembly. *Biotechnology Advances*, *20*, 321–339.

75. Zemb, T., & Blume, A. (2003). Self-assembly: weak and specific intermolecular interactions at work. *Current Opinion in Colloid & Interface Science*, *8*(1), 1–4.

76. Claessens, C. G., & Stoddart, J. F. (1997). π-π interactions in self-assembly. *Journal of Physical Organic Chemistry*, *10*, 254–272.

77. Ulijn, R. V, & Smith, A. M. (2008). Designing peptide based nanomaterials. *Chemical Society Reviews*, *37*(4), 664–75.

78. Yang, Z., Wang, J., Xu, B., Gao, P., & Wang, L. (2010). Phenyl groups in supramolecular nanofibers confer hydrogels with high elasticity and rapid recovery. *Journal of Materials Chemistry*, *11*(20), 2128-2132.

79. Xu, H., Das, A. K., Horie, M., Shaik, M. S., Smith, A. M., Luo, Y., & Ulijn, R. V. (2010). An investigation of the conductivity of peptide nanotube networks prepared by enzyme-triggered self-assembly. *Nanoscale*, *2*(6), 960–6.

80. Buckingham, A. D., Fowler, P. W., & Hutson, J. M. (1988). Theoretical studies of van der Waals molecules and intermolecular forces. *Chemical Reviews*, *88*, 963–988.

81. Zhang, S. (2003). Building from the bottom up. *Materials Today*, 6, 20-27.

82. Liu, Y., Kim, E., Ulijn, R. V., Bentley, W. E., & Payne, G. F. (2011). Reversible electroaddressing of self-assembling amino-acid conjugates. *Advanced Functional Materials*, *21*, 1575–1580.

83. Biesalski, M. A., Knaebel, A., Tu, R., & Tirrell, M. (2006). Cell adhesion on a polymerized peptide-amphiphile monolayer. *Biomaterials*, *27*, 1259–1269.

84. Smith, K. H., Tejeda-Montes, E., Poch, M., & Mata, A. (2011). Integrating top-down and self-assembly in the fabrication of peptide and protein-based biomedical materials. *Chemical Society Reviews*, *40*, 4563–4577.

85. Arosio, P., Owczarz, M., Wu, H., Butté, A., & Morbidelli, M. (2012b). End-to-end self-assembly of RADA 16-I nanofibrils in aqueous solutions. *Biophysical Journal*, *102*(7), 1617–26.

86. Shigemasa, Y., & Minami, S. (1996). Applications of chitin and chitosan for biomaterials. *Biotechnology and Genetic Engineering Reviews*, *13*(1), 383–420.

87. Gelain, F., Bottai, D., Vescovi, A., & Zhang, S. (2006). Designer self-assembling peptide nanofiber scaffolds for adult mouse neural stem cell 3-dimensional cultures. *PloS One*, *1*(1), 119.

88. Schachner, M. (2000). Neurobiology: nervous engineering. *Nature*, *405*(6788), 747-748.

89. Nagai, Y., Unsworth, L. D., Koutsopoulos, S., & Zhang, S. (2006). Slow release of molecules in self-assembling peptide nanofiber scaffold. *Journal of Controlled Release : Official Journal of the Controlled Release Society*, *115*(1), 18–25.

90. Gelain, F., Unsworth, L. D., & Zhang, S. (2010). Slow and sustained release of active cytokines from self-assembling peptide scaffolds. *Journal of Controlled Release : Official Journal of the Controlled Release Society*, *145*(3), 231–9.

91. Liu, J., Zhang, L., Yang, Z., & Zhao, X. (2011). Controlled release of paclitaxel from a self-assembling peptide hydrogel formed in situ and antitumor study in vitro. *International Journal of Nanomedicine*, *6*, 2143–53.

92. Koutsopoulos, S., Unsworth, L. D., Nagai, Y., & Zhang, S. (2009). Controlled release of functional proteins through designer self-assembling peptide nanofiber hydrogel scaffold. *Proceedings of the National Academy of Sciences of the United States of America*, *106*(12), 4623–8.

93. Davis, M. E., Hsieh, P. C. H., Takahashi, T., Song, Q., Zhang, S., Kamm, R. D., & Lee, R. T. (2006). Local myocardial insulin-like growth factor 1 (IGF-1) delivery with biotinylated peptide nanofibers improves cell therapy for myocardial infarction. *Proceedings of the National Academy of Sciences of the United States of America*, *103*(21), 8155–60.

94. Holmes, T. C., de Lacalle, S., Su, X., Liu, G., Rich, a, & Zhang, S. (2000). Extensive neurite outgrowth and active synapse formation on self-assembling peptide scaffolds. *Proceedings of the National Academy of Sciences of the United States of America*, *97*(12), 6728–33

95. Semino, C. E., Merok, J. R., Crane, G. G., Panagiotakos, G., & Zhang, S. (2003). Functional differentiation of hepatocyte-like spheroid structures from putative liver progenitor cells in three-dimensional peptide scaffolds. *Differentiation; Research in Biological Diversity*, *71*(4-5), 262–70.

96. Semino, C. E., Kasahara, J., & Hayashi, Y. (2004). Entrapment of migrating hippocampal neural cells in three-dimensional peptide nanofiber scaffold. *Tissue Eng.*, *10*(3), 643-55.

97. Bokhari, M. A., Akay, G., Zhang, S., & Birch, M. A. (2005). The enhancement of osteoblast growth and differentiation in vitro on a peptide hydrogel-polyHIPE polymer hybrid material. *Biomaterials*, *26*, 5198–5208.

98. Horii, A., Wang, X., Gelain, F., & Zhang, S. (2007). Biological designer self-assembling peptide nanofiber scaffolds significantly enhance osteoblast proliferation, differentiation and 3-D migration. *PloS One*, *2*(2), 190.

99. Thonhoff, J. R., Lou, D. I., Jordan, P. M., Zhao, X., & Wu, P. (2008). Compatibility of human fetal neural stem cells with hydrogel biomaterials in vitro. *Brain Research*, *1187*, 42–51.

100. Kao, B., Kadomatsu, K., & Hosaka, Y. (2009). Construction of synthetic dermis and skin based on a self-assembled peptide hydrogel scaffold. *Tissue Engineering. Part A*, *15*, 2385–2396.

101. Wang, T., Zhong, X., Wang, S., Lv, F., & Zhao, X. (2012). Molecular mechanisms of RADA16-1 peptide on fast stop bleeding in rat models. *International Journal of Molecular Sciences*, *13*, 15279–90.

102. Wen, Z., Hu, Y. A., Liao, Q., & Zhao, Y. (2013). The self assembly peptide RADA16-1 suppreses the malignant phenotype of pancreatic cancer cell line MIAPaCa-2 in three-dimensional culture and in vivo, *8*(1), 281–290.

103. Moradi, F., Bahktiari, M., Joghataei, M. T., Nobakht, M., Soleimani, M., Hasanzadeh, G., & Maleki, F. (2012). BD PuraMatrix peptide hydrogel as a culture system for human fetal Schwann cells in spinal cord regeneration. *J Neurosci Res*, *90*, 2335–2348.

104. Kakiuchi, Y., Hirohashi, N., & Murakami-Murofushi, K. (2013). The macroscopic structure of RADA16 peptide hydrogel stimulates monocyte/macrophage differentiation in HL60 cells via cholesterol synthesis. *Biochemical and Biophysical Research Communications*, *433*(3), 298–304.

105. Tokunaga, M., Liu, M.-L., Nagai, T., Iwanaga, K., Matsuura, K., Takahashi, T., & Komuro, I. (2010). Implantation of cardiac progenitor cells using self-assembling peptide improves cardiac function after myocardial infarction. *Journal of Molecular and Cellular Cardiology*, *49*(6), 972–83.

106. Patel, D. M., Shah, J., & Srivastava, A. S. (2013). Therapeutic potential of mesenchymal stem cells in regenerative medicine. *Stem Cells Int., 2013*, 1-15.

107. McNamara, L. E., McMurray, R. J., Biggs, M. J. P., Kantawong, F., Oreffo, R. O. C., & Dalby, M. J. (2010). Nanotopographical control of stem cell differentiation. *Journal of Tissue Engineering, 2010*, 120623.

108. Engler, A. J., Sen, S., Sweeney, H. L., & Discher, D. E. (2006). Matrix elasticity directs stem cell lineage specification. *Cell*, *126*(4), 677–89.

109. Dalby, M. J., Gadegaard, N., Tare, R., Andar, A., Riehle, M. O., Herzyk, P., & Oreffo, R. O. C. (2007). The control of human mesenchymal cell differentiation using nanoscale symmetry and disorder. *Nature Materials*, *6*(12), 997–1003.

110. Hamada, K., Hirose, M., Yamashita, T., & Ohgushi, H. (2008). Spatial distribution of mineralized bone matrix produced by marrow mesenchymal stem cells in self-assembling peptide hydrogel scaffold. *Journal of Biomedical Materials Research. Part A*, *84*, 128–136.

111. Erickson, I. E., Huang, A. H., Chung, C., Li, R. T., Burdick, J. A., & Mauck, R. L. (2009). Differential maturation and structure-function relationships in mesenchymal stem cell- and chondrocyte-seeded hydrogels. *Tissue Eng Part A*, *15*(5), 1041-52.

112. Yoshimi, R., Yamada, Y., Ito, K., Nakamura, S., Abe, A., Nagasaka, T., & Ueda, M. (2009). Self-assembling peptide nanofiber scaffolds, platelet-rich plasma, and mesenchymal stem cells for injectable bone regeneration with tissue engineering. *The Journal of Craniofacial Surgery*, *20*, 1523–1530.

113. Matsumoto, T., Tadokoro, M., Hattori, K., Ougushi, H., & Satou, J. (2011). Osteogenic differentiation of mesenchymal stem cells/polymer composites with HA in vitro. *Bioceramics Development and Applications*, *1*, 1–4.

114. Chen, K., Eng, B., Sahoo, S., Ph, D., He, P., Ng, K. S., & Goh, J. C. H. (2012). A hybrid silk / RADA-based fibrous scaffold with triple hierarchy for ligament regeneration, *18* (13-14), 1399-409.

115. Chen, J., Shi, S.D., Xinying J.I., Morales, G., Jingwei, Z., Navneet, K., & Sihong, W. (2013). Enhanced osteogenesis of human mesenchymal stem cells by periodic heat shock. *Tissue Eng Part A*, *19*(5), 716–728.

116. Mansur, H. S., Oréfice, R. L., & Mansur, A. A. P. (2004). Characterization of poly(vinyl alcohol)/ poly(ethylene glycol) hydrogels and PVA-derived hybrids by small-angle X-ray scattering and FTIR spectroscopy. *Polymer*, *45*(21), 7193–7202.

117. Roy, S., Javid, N., Sefcik, J., Halling, P. J., & Ulijn, R. V. (2012). Salt-induced control of supramolecular order in biocatalytic hydrogelation. *Langmuir : The ACS Journal of Surfaces and Colloids*, *28*(48), 16664–70.

118. Coviello, T., Coluzzi, G., Palleschi, A., Grassi, M., Santucci, E., & Alhaique, F. (2003). Structural and rheological characterization of scleroglucan/ borax hydrogel for drug delivery. *International Journal of Biological Macromolecules*, *32*(3-5), 83–92.

119. Omari, A., Tabary, R., Rousseau, D., Calderon, F. L., Monteil, J., & Chauveteau, G. (2006). Soft water-soluble microgel dispersions: structure and rheology. *Journal of Colloid and Interface Science*, *302*(2), 537–46.

120. Al-Assaf, S., Phillips, G. O., Aoki, H., & Sasaki, Y. (2007). Characterization and properties of Acacia senegal (L.) Willd. var. senegal with enhanced properties (Acacia (sen) SUPER GUM™): Part 1—Controlled maturation of Acacia senegal var. senegal to increase viscoelasticity, produce a hydrogel form and convert a poor into a good emulsifier. *Food Hydrocolloids*, *21*(3), 319–328.

121. Roy, S., Javid, N., Frederix, P. W. J. M., Lamprou, D. a, Urquhart, A. J., Hunt, N. T., & Ulijn, R. V. (2012). Dramatic specific-ion effect in supramolecular hydrogels. *Chemistry (Weinheim an Der Bergstrasse, Germany)*, *18*(37), 11723–31.

122. Duygu, D. Y., Baykal, T., Açikgöz, İ., & Yildiz, K. (2009). Review: Fourier transform infrared (FT-IR) spectroscopy for biological studies. *Gazi University Journal of Science*, *22*, 117–121.

123. Kong, J., & Yu, S. (2007). Fourier transform infrared spectroscopic analysis of protein secondary structures protein FTIR data analysis and band assignment, *Acta Biochimica et Biophysica Sinica* , *39*(8), 549–559.

124. Barth, A., & Zscherp, C. (2002). What vibrations tell about proteins. *Quarterly Reviews of Biophysics*, *35*(4), 369–430.

125. Pelton, J. T., & McLean, L. R. (2000). Spectroscopic methods for analysis of protein secondary structure. *Analytical Biochemistry*, *277*, 167–76.

126. Plum, E., Liu, X.-X., Fedotov, V. A., Chen, Y., Tsai, D. P., & Zheludev, N. I. (2009). Metamaterials: optical activity without chirality. *Physical Review Letters*, *102*, 113902.

127. Kelly, S. M., & Price, N. C. (2000). The use of circular dichroism in the investigation of protein structure and function. *Current Protein & Peptide Science*, *1*(4), 349–84.

128. Parson, W. W. (2007). *Modern optical spectroscopy*. New York, USA: Springer.

129. Kelly, S. M., Jess, T. J., & Price, N. C. (2005). How to study proteins by circular dichroism. *Biochimica et Biophysica Acta - Proteins and Proteomics*, *1751*(2), 119–139.

130. Gross, L. (2011). Recent advances in submolecular resolution with scanning probe microscopy. *Nature Chemistry*, *3*, 273–278.

131. Müller, D. J., & Dufrêne, Y. F. (2011). Atomic force microscopy: a nanoscopic window on the cell surface. *Trends in Cell Biology*, *21*(8), 461–9.

132. Pittenger, B., Erina, N., & Su, C. (2014). Mechanical property mapping at the nanoscale using peak force QNM scanning probe technique. *Nanomechanical Analysis of High Performance Materials*, *203*, 31–51.

133. Garside, P., Mills, G., Smith, J., & Wyeth, P. (2014). An investigation of weighted and degraded silk by complementary microscopy techniques. *E-Preservation Science*, *11*, 15–21.

134. Jalili, N., & Laxminarayana, K. (2004). A review of atomic force microscopy imaging systems: application to molecular metrology and biological sciences. *Mechatronics*, *14*(8), 907–945.

135. Song, Y., & Bhushan, B. (2008). Atomic force microscopy dynamic modes: modeling and applications. *Journal of Physics: Condensed Matter*, *20*(22), 225012.

136. Zhong, Q., Inniss, D., Kjoller, K., & Elings, V. B. (1993). Fractured polymer/ silica fiber surface studied by tapping mode atomic force microscopy. *Surface Science*, *290*, L688–L692.

137. Seo, Y., & Jhe, W. (2008). Atomic force microscopy and spectroscopy. *Reports on Progress in Physics*, *71*, 016101.

138. Pittenger, B., Slade, A., & Berquand, A. (2013). Toward quantitative nanomechanical measurements on live cells with peak-force QNM. *Bruker Application Note, AN141*, 1-10.

139. Pittenger, B. B., Erina, N., & Su, C. (1993). Quantitative mechanical property mapping at the nanoscale with peak-force QNM. *Nanoscale Research Letters, 6, 70.*

140. Castillo-león, J., Andersen, K. B., & Svendsen, W. E. (n.d.). Self –assembled peptide nanostructures for biomedical applications : advantages and challenges. *Biomaterials Science and Engineering, 5,* 115-134.

141. Oswald, J., Boxberger, S., Jørgensen, B., Feldmann, S., Ehninger, G., Bornhäuser, M., & Werner, C. (2004). Mesenchymal stem cells can be differentiated into endothelial cells in vitro. *Stem Cells, 22,* 377–384.

142. Lo Nostro, P., & Ninham, B. W. (2012). Hofmeister phenomena: an update on ion specificity in biology. *Chemical Reviews, 112*(4), 2286–322.

143. Affenzeller, M. J., Darehshouri, A., Andosch, A., Lütz, C., & Lütz-Meindl, U. (2009). Salt stress-induced cell death in the unicellular green alga Micrasterias denticulata. *Journal of Experimental Botany, 60,* 939–954.

144. Salis, A., Bilanicova, D., Ninham, B. W., & Monduzzi, M. (2007). Hofmeister effects in enzymatic activity: weak and strong electrolyte influences on the activity of Candida rugosa lipase. *The Journal of Physical Chemistry. B, 111*, 1149–1156.

145. Collins, K. D. (2004). Ions from the Hofmeister series and osmolytes: Effects on proteins in solution and in the crystallization process. *Methods, 34,* 300–311.

146. Lo Nostro, P., Ninham, B. W., Lo Nostro, A., Pesavento, G., Fratoni, L., & Baglioni, P. (2005). Specific ion effects on the growth rates of Staphylococcus aureus and Pseudomonas aeruginosa. *Physical Biology, 2,* 1–7.

147. Parsons, D. F., Boström, M., Lo Nostro, P., & Ninham, B. W. (2011). Hofmeister effects: interplay of hydration, nonelectrostatic potentials, and ion size. *Physical Chemistry Chemical Physics, 13*(27), 12352–67.

148. Zhang, Y., & Cremer, P. S. (2006). Interactions between macromolecules and ions: The Hofmeister series. *Current Opinion in Chemical Biology, 10*(6), 658–63.

149. Caplan, M. R., Moore, P. N., Zhang, S., Kamm, R. D., & Lauffenburger, D. A. (2000). Self-assembly of a beta-sheet protein governed by relief of electrostatic repulsion relative to van der Waals attraction. *Biomacromolecules, 1,* 627–631.

150. Caplan, M. R., Schwartzfarb, E. M., Zhang, S., Kamm, R. D., & Lauffenburger, D. A. (2002). Control of self-assembling oligopeptide matrix formation through systematic variation of amino acid sequence. *Biomaterials*, *23*, 219–227.

151. Nesloney, C. L., & Kelly, J. W. (1996). Progress towards understanding beta-sheet structure. *Bioorganic & Medicinal Chemistry*, *4*, 739–766.

152. Jun, S., Hong, Y., Imamura, H., Ha, B.-Y., Bechhoefer, J., & Chen, P. (2004). Self-assembly of the ionic peptide EAK16: the effect of charge distributions on self-assembly. *Biophysical Journal*, *87*, 1249–1259.

153. Okombo, J., Kiara, S. M., Rono, J., Mwai, L., Pole, L., Ohuma, E., & Nzila, A. (2010). *In vitro* activities of quinine and other antimalarials and pfnhe polymorphisms in Plasmodium isolates from Kenya. *Antimicrobial Agents and Chemotherapy*, *54*, 3302–3307.

154. Dorn, A., Vippagunta, S. R., Matile, H., Jaquet, C., Vennerstrom, J. L., & Ridley, R. G. (1998). An assessment of drug-haematin binding as a mechanism for inhibition of haematin polymerisation by quinoline antimalarials. *Biochemical Pharmacology*, *55*, 727–736.

155. Orengo, J. M., Leliwa-Sytek, A., Evans, J. E., Evans, B., van de Hoef, D., Nyako, M., & Rodriguez, A. (2009). Uric acid is a mediator of the Plasmodium falciparum-induced inflammatory response. *PLoS ONE*, *4*(4), 5194- 5194.

156. Hallifax, D., & Houston, J. B. (2007). Saturable uptake of lipophilic amine drugs into isolated hepatocytes: mechanisms and consequences for quantitative clearance prediction. *Drug Metabolism and Disposition*, *35*, 1325–1332.

157. Avdeef, A., Box, K. J., Comer, J. E. A., Gilges, M., Hadley, M., Hibbert, C., & Tam, K. Y. (1999). pH-metric logP 11. pK(a) determination of water-insoluble drugs in organic solvent-water mixtures. *Journal of Pharmaceutical and Biomedical Analysis*, *20*, 631–641.

158. Sadeghi, M., & Hosseinzadeh, H. (2008). Synthesis of starch-poly(sodium acrylate-co-acrylamide) superabsorbent hydrogel with salt and pH-responsiveness properties as a drug delivery system. *Journal of Bioactive and Compatible Polymers*, *23*(4), 381–404.

159. Mains, J., Lamprou, D. a, McIntosh, L., Oswald, I. D. H., & Urquhart, A. J. (2013). Beta-adrenoceptor antagonists affect amyloid nanostructure; amyloid hydrogels as drug delivery vehicles. *Chemical Communications* , *49*(44), 5082–4.

160. Reznikoff, C. A., Brankow, D. W., & Heidelberger, C. (1973). Establishment and characterization of a cloned line of C3H mouse embryo cells sensitive to postconfluence inhibition of division, *Cancer Research*, *33*(12), 3231–3238.

161. Tang, Q.-Q., Otto, T. C., & Lane, M. D. (2004). Commitment of C3H10T1/2 pluripotent stem cells to the adipocyte lineage. *Proceedings of the National Academy of Sciences of the United States of America*, *101*(26), 9607–11.

162. Katagiri, T., Yamaguchi, A., Ikeda, T., Yoshiki, S., Wozney, J. M., Rosen, V., & Suda, T. (1990). The non-osteogenic mouse pluripotent cell line, C3H10T1/2, is induced to differentiate into osteoblastic cells by recombinant human bone morphogenetic protein-2. *Biochemical and Biophysical Research Communications*, *172*, 295–299.

163. Denker, a E., Haas, a R., Nicoll, S. B., & Tuan, R. S. (1999). Chondrogenic differentiation of murine C3H10T1/2 multipotential mesenchymal cells: I. stimulation by bone morphogenetic protein-2 in high-density micromass cultures. *Differentiation; Research in Biological Diversity*, *64*(2), 67–76.

164. Cheddadi, M., López-Cabarcos, E., Slowing, K., Barcia, E., & Fernández-Carballido, A. (2011). Cytotoxicity and biocompatibility evaluation of a poly(magnesium acrylate) hydrogel synthesized for drug delivery. *International Journal of Pharmaceutics*, *413*(1-2), 126–33.

165. Sen, A., Lea-Currie, Y. R., Sujkowska, D., Franklin, D. M., Wilkison, W. O., Halvorsen, Y. D., & Gimble, J. M. (2001). Adipogenic potential of human adipose derived stromal cells from multiple donors is heterogeneous. *Journal of Cellular Biochemistry*, *81*(2), 312–9.

166. Huang, H., Song, T.-J., Li, X., Hu, L., He, Q., Liu, M., & Tang, Q.-Q. (2009). BMP signaling pathway is required for commitment of C3H10T1/2 pluripotent stem cells to the adipocyte lineage. *Proceedings of the National Academy of Sciences of the United States of America*, *106*, 12670–12675.

167. Lee, J. S., Suh, J. M., Park, H. G., Bak, E. J., Yoo, Y.-J., & Cha, J.-H. (2008). Heparin-binding epidermal growth factor-like growth factor inhibits adipocyte differentiation at commitment and early induction stages. *Differentiation Research in Biological Diversity*, *76*(5), 478–87.

168. Lee, J. S., Park, J.-H., Kwon, I. K., & Lim, J. Y. (2011). Retinoic acid inhibits BMP4-induced C3H10T1/2 stem cell commitment to adipocyte via downregulating Smad/p38MAPK signaling. *Biochemical and Biophysical Research Communications*, *409*(3), 550–5.

169. Zhao, L., Li, G., Chan, K.-M., Wang, Y., & Tang, P.-F. (2009). Comparison of multipotent differentiation potentials of murine primary bone marrow stromal cells and mesenchymal stem cell line C3H10T1/2. *Calcified Tissue International*, *84*(1), 56–64.

170. Cho, S. W., Her, S. J., Sun, H. J., Choi, O. K., Yang, J.-Y., Kim, S. W., & Shin, C. S. (2008). Differential effects of secreted frizzled-related proteins (sFRPs) on osteoblastic differentiation of mouse mesenchymal cells and apoptosis of osteoblasts. *Biochemical and Biophysical Research Communications*, *367*(2), 399–405.

171. Bone, P., Nude, O., & Yang, J. (2013). Transplantation of human umbilical cord blood-derived mesenchymal stem cells or their conditioned medium prevents bone loss in ovariectomized nude mice. *Tissue Eng Part A, 19*(5). 685-696.

172. Al-Nasiry, S., Geusens, N., Hanssens, M., Luyten, C., & Pijnenborg, R. (2007). The use of Alamar blue assay for quantitative analysis of viability, migration and invasion of choriocarcinoma cells. *Human Reproduction*, *22*, 1304–1309.

173. Ruoslahti, E. (1984). Fibronectin in cell adhesion and invasion. *Cancer Metastasis Reviews*, *3*, 43–51.

174. Yamamoto, S., Tanaka, M., Sunami, H., Arai, K., Takayama, A., Yamashita, S., & Shimomura, M. (2006). Relationship between adsorbed fibronectin and cell adhesion on a honeycomb-patterned film. *Surface Science*, *600*, 3785–3791.

175. Chandar, N., & Viselli, S. (2010). *Cell and molecular biology*. Philadelphia, USA: Lippincott Williams & Wilkins.

176. Seo, C. H., Jeong, H., Feng, Y., Montagne, K., Ushida, T., Suzuki, Y., & Furukawa, K. S. (2014). Micropit surfaces designed for accelerating osteogenic differentiation of murine mesenchymal stem cells via enhancing focal adhesion and actin polymerization. *Biomaterials*, *35*, 2245–2252.

177. Inagaki, Y., Kitamura, N., Kurokawa, T., Tanaka, Y., Gong, J. P., Yasuda, K., & Tohyama, H. (2014). Effects of culture on PAMPS/PDMAAm double-network gel on chondrogenic differentiation of mouse C3H10T1/2 cells: in vitro experimental study. *BMC Musculoskeletal Disorders*, *15*(1), 320.